https://doi.org/10.5194/egusphere-2026-4891
Preprint. Discussion started: 28 September 2026

Physical controls on North Atlantic organic carbon export from eddying ocean models

Xi Ruan[1], Stéphane Doléac[2,3], Laurent Bopp[2], Julian Mak[1,4], Franziska U. Schwarzkopf[5], Arne Biastoch[5,6], and Marina Lévy[2]

[1]Department of Ocean Science, Hong Kong University of Science and Technology, Hong Kong
[2]Laboratoire d'Océanographie et du Climat: Expérimentations et Analyses Numériques de l'Institut Pierre Simon Laplace (LOCEAN-IPSL) - Sorbonne Université, CNRS, IRD, MHNH, Paris, France
[3]École des Ponts, Marne-la-Vallée, France
[4]National Centre of Oceanography, Southampton, United Kingdom
[5]GEOMAR Helmholtz Centre for Ocean Research Kiel, Kiel, Germany
[6]Christian-Albrechts Universität zu Kiel, Kiel, Germany

Correspondence: Xi Ruan (xruana@ust.hk) and Stéphane Doléac (stephane.doleac@locean.ipsl.fr)

Abstract. Organic carbon export from the surface mixed layer to the ocean interior is a central component of the biological carbon pump, yet physically driven subduction export of particulate and dissolved organic carbon (POC and DOC, respectively) remains poorly constrained. The North Atlantic is a critical region for organic carbon export, where strong physical and biological contrasts generate substantial spatial and temporal variability in export pathways. Here, we employ an eddy-present global ocean–sea ice model configuration with an embedded eddy-rich Atlantic to quantify the spatial and temporal variability of subduction export in the North Atlantic and to evaluate its sensitivity to model resolution. We divide total organic carbon export into gravitationally driven sedimentation export and physically driven subduction export, the latter comprising advective and mixed-layer exports. Regionally, subduction export contributes up to 34 % of total POC export across the examined bioregions (from south to north: subtropical, intermediate, subpolar, and ice-covered regions) and is consistently partitioned between advective and mixed-layer export in an ∼2:1 ratio except in the ice-covered region; total DOC export is also dominated by the advective component within subduction, accounting for up to 94 %. This broadly uniform partitioning persists despite the pronounced south-to-north patterns in the net export fluxes of both total POC and DOC. Seasonally, a winter–spring peak in advective export precedes the spring maximum in mixed-layer export, and is followed by a spring–summer maximum in sedimentation export in most regions, a pattern common to both POC and DOC, indicating a first-order role of subduction export alongside sedimentation export in shaping seasonal carbon export. Comparison between eddy-present and eddy-rich simulations shows generally higher export for both tracers in the eddy-rich simulation, with differences peaking at mid-to-high latitudes and reaching up to 64 % of the eddy-rich export for DOC in the ice-covered region. The advective component is particularly sensitive to model resolution, underscoring the need to better resolving the physical processes that regulate subduction export. Together, these results provide a further constraint on physically driven subduction export in the North Atlantic and a stronger basis for understanding its role in ocean carbon cycling.

https://doi.org/10.5194/egusphere-2026-4891
Preprint. Discussion started: 28 September 2026

1 Introduction

Organic carbon export, the transfer of particulate and dissolved organic carbon (POC and DOC, respectively) from the surface mixed layer into the ocean interior, is a central component of the biological carbon pump and enables the sequestration of atmospheric CO_2 on timescales from years to millennia (Volk and Hoffert, 1985; Falkowski et al., 2000; Nowicki et al., 2022, 2024). This export occurs through multiple pathways, including the gravitational sinking of POC (driven by particle settling), biologically mediated transfer (through animal migration), and physically driven subduction export (arising from ocean circulation and mixing), with the latter two pathways transferring both POC and DOC across the mixed-layer base (Boyd et al., 2019; Siegel et al., 2023). Among these pathways, gravitational sinking accounts for $\sim 4-9\,\mathrm{Pg\,C\,yr^{-1}}$ of global export (Henson et al., 2011; Bopp et al., 2013; Siegel et al., 2014; DeVries and Weber, 2017) and has long been recognised as the dominant pathway, remaining the most extensively studied and best constrained (Berelson, 2001; Nowicki et al., 2022; Fox et al., 2024; Romanelli et al., 2024). This is largely because POC produces vertically directed fluxes that can be measured locally and directly, allowing observations using sediment traps (Martin et al., 1987; Honjo and Manganini, 1993), thorium isotope measurements (Le Moigne et al., 2013; Lemaitre et al., 2018), autonomous optical and imaging platforms (Bishop, 2009; Guidi et al., 2015), and satellite observations combined with models (Siegel et al., 2014). Biologically mediated transfer, in turn, accounts globally for $\sim 1.2-4.6\,\mathrm{Pg\,C\,yr^{-1}}$ (Davison et al., 2013; Jónasdóttir et al., 2015) and represents an important pathway, with estimates increasingly constrained through direct quantification using targeted observations such as midwater trawls (Childress et al., 1980; Davison et al., 2013), acoustic surveys (Powell and Ohman, 2012; Bianchi et al., 2013), and biomass-based measurements (Giering et al., 2017), as well as through indirect constraints from geochemical tracers, for example by relating oxygen consumption to remineralisation (Jónasdóttir et al., 2015).

In contrast, physically driven subduction export remains much less certain (Sanders et al., 2014; Lacour et al., 2019; Le Moigne, 2019), despite the growing recognition of its importance (Stramska, 2010; Karleskind et al., 2011; Fontela et al., 2016; Giering et al., 2016; Dall'Olmo et al., 2016; Bol et al., 2018; Johnson and Omand, 2021; Wang and Fennel, 2022; Bellacicco et al., 2025). Two primary mechanisms contribute to subduction export: the advective pump, through which ocean circulation and mixing transport organic material across the mixed-layer base, and the mixed-layer pump, whereby organic carbon produced and accumulated during the growing season is mixed downward and subsequently isolated below the mixed layer during restratification (Boyd et al., 2019; Siegel et al., 2023). In this framework, the advective pump is defined inclusively to encompass transport by the mean circulation and, where available, eddy subduction pump, which can be explicitly represented in high-resolution frameworks (Omand et al., 2015; Boyd et al., 2019; Resplandy et al., 2019). These two primary mechanisms are difficult to observe directly because organic carbon is transported within moving water masses across multiple spatial dimensions rather than as a strictly vertical flux, and the mixed-layer base is sloped and highly time-varying (Lévy et al., 2013). In addition, coordinated physical and biogeochemical measurements at the relevant spatial and temporal scales are rarely available, and the spatial-temporal decoupling of these processes in the real ocean further complicates interpreta-

https://doi.org/10.5194/egusphere-2026-4891
Preprint. Discussion started: 28 September 2026

tion (McGillicuddy et al., 2019; Johnson et al., 2024). Multiple pathways often act simultaneously, complicating efforts to disentangle individual transport pathways (Boyd et al., 2019). Furthermore, their high sensitivity to mesoscale (10–100 km) and submesoscale variability (1–10 km), vertical mixing, and stratification can also lead to substantial uncertainty (Sanders et al., 2014; Omand et al., 2015; Lévy et al., 2018; Resplandy et al., 2019; Hewitt et al., 2020, 2022). Nevertheless, despite these uncertainties, current estimates of $\sim 0.1-0.5\,\mathrm{PgC\,yr^{-1}}$ for the mixed-layer pump (Bishop et al., 1986; Dall'Olmo et al., 2016) and up to $\sim 2.1\,\mathrm{PgC\,yr^{-1}}$ for advective pump (Lévy et al., 2013; Omand et al., 2015) indicates that these processes may constitute an important component of carbon export. Consequently, as constraints on gravitational sinking and biologically mediated transfer continue to improve, physically driven subduction export requires a more robust quantification.

The North Atlantic is one of the most important regions for global organic carbon export, and large contrasts in physical and biological conditions across the basin are associated with strong spatial and temporal variability in export (Henson et al., 2012; Siegel et al., 2014; Sanders et al., 2014; DeVries and Weber, 2017; Baker et al., 2022). In the subtropical gyre, oligotrophic waters limit biological production and result in weak export (McClain et al., 2004; Leonelli et al., 2022). In western boundary current regions, energetic currents enhance lateral stirring and vertical exchange, increasing the transport of organic carbon (Haëck et al., 2023; Gray et al., 2024). Farther north, in the subpolar region, deep winter mixed layers produce strong seasonal cycles in both biological production and organic carbon export (Palevsky and Nicholson, 2018; Fogaren et al., 2025). At higher latitudes, seasonal sea-ice cover leads to shallow mixed layers and intermittent export events (von Appen et al., 2021; Chen et al., 2025). However, poor constraints on physically driven subduction export limit our ability to quantify its role in shaping the variability of organic carbon export in the North Atlantic and, given its central role in the global ocean carbon cycle, remain a source of uncertainty in estimates of global carbon budgets and climate projections.

This study aims to quantify the contribution of physically driven subduction export to total POC and DOC exports in the North Atlantic within a modelling framework. We employ an eddy-present global ocean–sea ice circulation model with an eddy-rich refinement in the Atlantic that is capable of resolving mesoscale eddies. Our analysis is guided by three key questions: (1) What is the spatial distribution of subduction export among the major bioregions of the North Atlantic basin, namely, from south to north, the subtropical, intermediate, subpolar, and ice-covered regions? (2) How does subduction export vary on monthly timescales within the basin and across these bioregions? (3) How sensitive are the export pathways to model resolution, as revealed by differences between the eddy-rich and an eddy-present configuration?

To ensure terminological clarity, we use consistent terms for describing organic carbon export across the mixed-layer base. Previous studies have used varied terms, such as gravitational pump, subduction pump, and particle-injection pump, with "pump" referring to subduction of organic carbon despite its broader definition encompassing both subduction of organic carbon and obduction of remineralised dissolved inorganic carbon (Boyd et al., 2019; Resplandy et al., 2019). To avoid this ambiguity and to focus specifically on the subduction and gravitational sinking of organic carbon across the mixed-layer base, we use the following explicit terms throughout this study, noting that biologically mediated transfer is not represented in our modeling framework (cf. Sect. 2.1): *subduction export* refers to all physically driven exports of POC and DOC, *sedimentation export* denotes the gravitational sinking of POC. For diagnostic purposes, subduction export is further separated into *advective export* and *mixed-layer export*, corresponding to the advective pump and mixed-layer pump, respectively. Note that export here

https://doi.org/10.5194/egusphere-2026-4891
Preprint. Discussion started: 28 September 2026

refers to the net exchange of organic carbon across the mixed-layer boundary, encompassing both influx of organic carbon from the mixed layer into the ocean interior and its efflux from the interior back to the mixed layer (cf. Fig. 1b,c,e,f); sedimentation export is restricted to influx by definition, whereas subduction export includes both.

The following section (Sect. 2) describes the model simulations, the definition of the bioregions, and the diagnostic framework. We then present the results addressing the three guiding questions (Sect. 3). The paper ends with a discussion of the results and limitations (Sect. 4) and a summary of the main findings (Sect. 5).

2 Method

2.1 Model simulations

To quantify the pathways driving organic carbon export in the North Atlantic, we employ two global ocean–sea ice model configurations:

- ORCA025: an eddy-present global configuration with a nominal horizontal resolution of $1/4°$ (Barnier et al., 2006),
- VIKING20X: a nested global configuration with an eddy-rich Atlantic at a nominal resolution of $1/20°$ embedded into the ORCA025 grid (Biastoch et al., 2021).

The simulations in both configurations are based on the Nucleus for European Modelling of the Ocean (NEMO, version 3.6; Madec et al. 2016) coupled with the Louvain Neuve Ice Model (LIM2; Fichefet and Maqueda 1997). Biogeochemical processes are represented by the Pelagic Interactions Scheme for Carbon and Ecosystem Studies version 2 (PISCES-v2; Aumont et al. 2015a). The physical model configurations and the coupled biogeochemical model have been well documented in previous studies; therefore, only a brief overview is provided here.

The ORCA025 configuration is one of the standard global configurations in the NEMO modelling system, widely used in global ocean and climate research as a robust eddy-present modelling framework. It employs an orthogonal curvilinear, quasi-isotropic tripolar grid with a nominal horizontal resolution of $1/4°$. The present simulation employs a vertical discretisation consisting of 46 unevenly levels in z coordinate (partial steps enabled), with thickness ranging from $6\,\mathrm{m}$ near the surface to $\sim 250\,\mathrm{m}$ at depth, and a time-step size of 18 minutes.

The VIKING20X configuration provides a higher resolution than ORCA025 in the Atlantic, enabling a more realistic representation of ocean dynamics. It has been widely applied in previous studies and has demonstrated skill in representing large-scale and mesoscale variability (Rühs et al., 2021; Biastoch et al., 2021; Böning et al., 2023; Fraser et al., 2024; Schiller-Weiss et al., 2025; Schulzki et al., 2025). The configuration consists of an Atlantic nest, embedded as child grid at $1/20°$ resolution into the global ORCA025 parent grid at $1/4°$ resolution, through the adaptive grid refinement in Fortran (AGRIF; Debreu et al. 2008). The nest domain spans around $100°\,\mathrm{W}$–$20°\,\mathrm{E}$ and $33.5°\,\mathrm{S}$–$65°\,\mathrm{N}$ (northward to $69.3°\,\mathrm{N}$), with boundaries shaped by the tripolar coordinate system (cf. Fig. 1 in Biastoch et al. 2021). For the simulation considered here, the child grid employs the same vertical discretisation as the parent grid but uses a 5-minutes integration time step (15 minutes on the parent grid).

https://doi.org/10.5194/egusphere-2026-4891
Preprint. Discussion started: 28 September 2026

The physical circulation model is coupled the PISCES-v2 biogeochemical model, which is employed using its standard reference configuration and is run online with the physical models. It represents lower trophic levels and biogeochemical cycles of carbon and main nutrients through 24 prognostic tracers, including nanophytoplankton and diatoms (PHY, PHY2), microzooplankton and mesozooplankton (ZOO, ZOO2), dissolved organic carbon (DOC), small and large sinking particles (POC, GOC), nutrients, calcite ($\mathrm{CaCO_3}$), dissolved inorganic carbon (DIC), and oxygen ($\mathrm{O_2}$). In this study, we focus on DOC and the living and nonliving particulate compartments (PHY, PHY2, ZOO, ZOO2, POC, GOC) that together form POC. Note that DOC is represented as a semi-labile pool (typically $\sim 10-30\,\mu\mathrm{mol\,kg^{-1}}$ in stratified surface waters) in the model and does not explicitly encompass the rapidly cycled labile fraction (on the order of $\sim 1-10\,\mu\mathrm{mol\,kg^{-1}}$ in the sunlit layer), which is implicitly remineralised, nor the large refractory pool ($\sim 30-40\,\mu\mathrm{mol\,kg^{-1}}$ throughout the ocean interior), which is treated as a non-dynamic background reservoir (Hansell and Orellana, 2021). Consequently, the modelled DOC captures only the more export-relevant fraction and underrepresents both short-lived variability and long-term carbon storage; this limitation will be revisited in the discussion section.

Table 1 summarises the key settings of the simulations performed with the ORCA025 and VIKING20X configurations. The physical component of the simulations is initialised at rest in model year 1958 with temperature and salinity from the World Ocean Atlas 2013 (WOA13; Locarnini et al. 2013; Zweng et al. 2013). Atmospheric forcing and river runoff are prescribed from the JRA55-do reanalysis (version 1.4; Tsujino et al. 2018). The biogeochemical model is coupled online with the physical model, and biogeochemical tracers are initialised from the previously developed B1870-ORCA025 simulation of Terhaar et al. (2019). The ORCA025 simulation is integrated for 64 model years to 2022, while the VIKING20X simulation, owing to its substantially higher computational cost, is spun up for only 20 years to 1978.

Configuration	ORCA025	VIKING20X
Simulation	ORCA025.L46-KFS006-P-V	VIKING20X.L46-KFS007-Pa
Horizontal resolution	$1/4°$	$1/20°$
Time step	18 mins	5 mins (15 mins on the parent grid)
Momentum advection	Vector form with Hollingsworth correction	Vector form with Hollingsworth correction
Tracer advection	TVD scheme	TVD scheme
Momentum diffusion	Geopotential bi-Laplacian ∇^4, $-15\times10^{10}\,\mathrm{m^4\,s^{-1}}$	Geopotential bi-Laplacian ∇^4, $-1.2\times10^{9}\,\mathrm{m^4\,s^{-1}}$
Tracer diffusion	Iso-neutral Laplacian ∇^4, $300\,\mathrm{m^2\,s^{-1}}$	Iso-neutral Laplacian ∇^4, $60\,\mathrm{m^2\,s^{-1}}$
Simulation period	1958–2022	1958–1978

Table 1. Key settings for simulations in ORCA025 and VIKING20X.

The resulting simulations are denoted ORCA025.L46-KFS006-P-V ($1/4°$ hereafter) and VIKING20X.L46-KFS007-Pa ($1/20°$ hereafter). The former is similar to the ORCA025-JRA-OMIP experiment described in Biastoch et al. (2021), whereas the latter is based on the VIKING20X-JRA-OMIP simulation reported in the same study but employs refined momentum viscosity (cf. Table 1) and no-slip lateral boundary conditions near Cat Island ($24.4°\,\mathrm{N}$, $75.5°\,\mathrm{W}$) to stabilise the solution. For both simulations here, river input to the physical component is injected at the surface and at depth, while riverine nutrient input

https://doi.org/10.5194/egusphere-2026-4891
Preprint. Discussion started: 28 September 2026

to the biogeochemical component is omitted. Model performance is evaluated using variables relevant for constraining organic carbon export, showing overall good agreement with observations (Appendix A). Our analysis primarily relies on the eddy-rich $1/20°$ simulation, which reduces resolution-related biases, and is complemented by comparison with the eddy-present $1/4°$ simulation to assess the sensitivity of organic carbon export to model resolution. Results from the two simulations will be interpreted in the context of the corresponding simulations on which they are based.

All diagnostics are performed within the open ocean of the North Atlantic basin over the final 5 years shared by both simulations, from the start of 1974 to the end of 1978. The analysed subdomain is extracted from both simulations (Fig. 1a,d), bounded to the south at $\sim 8°\,\mathrm{N}$ and excluding marginal seas (Hudson Bay, Baltic Sea, and Mediterranean), the Pacific sector, and continental shelf regions shallower than $200\,\mathrm{m}$, to focus on open-ocean export. Over the diagnostic period, the circulation in the $1/20°$ simulation is considered to have reached a quasi-steady state, supported by the spin-up behaviour of the simulation on which it is based, which exhibited longer-term drifts particularly affecting deeper water masses, as evident from the long-term evolution of the Atlantic Meridional Overturning Circulation (Schiller-Weiss et al., 2025). Nevertheless, at the base of the mixed layer, the modelled POC and DOC export (as defined below) are close to statistical equilibrium in both the simulations analysed here, with weak deseasonalised drifts relative to the mean state ($< 3.5\%\,\mathrm{yr}^{-1}$). The corresponding total drift over the analysis period normalised by the seasonal amplitude is limited ($< 12.9\,\%$), indicating that residual spin-up effects are present but remain small compared with the seasonal cycle and that the simulated seasonal variability is reasonably represented.

2.2 Bioregions

To provide a consistent framework for spatial analysis within the North Atlantic basin, we divide the basin into bioregions — areas characterised by relatively homogeneous physical and biogeochemical conditions. The aim is to delineate the four major regimes: subtropical, intermediate, subpolar, and ice-covered regimes. The regionalisation is done with the combined self-organising map (SOM) and hierarchical agglomerative clustering (HAC) procedure (hereafter SOM + HAC; see Jouini et al. 2016 and El Hourany et al. 2021 for a detailed description). This procedure has already been applied in environmental sciences (Jouini et al., 2016; El Hourany et al., 2021; Baaklini et al., 2022), and its strength lies in its unsupervised clustering framework, which allows bioregions to emerge from intrinsic physical and biological patterns rather than being imposed a priori on the basis of predefined criteria. In our study, this property allows us to construct bioregions tailored to the $1/4°$ and $1/20°$ simulations, for investigating the underlying dynamics within each bioregion across simulations, and to observations, for assessing the model behaviour (cf. Appendix A).

Following Doléac et al. (2025), bioregions are first derived in the observations by applying the SOM + HAC procedure to the climatological seasonal cycles of five variables: sea-surface temperature (SST), sea-ice area fraction (ICE), mixed-layer depth (MLD), surface nitrate concentration (NO3), and surface chlorophyll concentration (CHL). The observational datasets are summarised in Table A1 and are selected to match the model simulations as closely as possible in terms of spatial coverage, temporal extent, and spatial resolution, thereby supporting both the subsequent application of the procedure to the model simulations and the evaluation of the simulations (cf. Appendix A). Nevertheless, CHL data coverage is incomplete spatially and temporally (cf. Fig. A1), but the procedure remains robust to missing data (Vatanen et al., 2015). These five fields are

https://doi.org/10.5194/egusphere-2026-4891
Preprint. Discussion started: 28 September 2026

first averaged across years to obtain monthly values, using the five diagnostic years when available in the observational data (i.e., SST), or otherwise the full observational reference period, except for the MLD and NO3 which are already monthly climatologies. When spatial resolution differs among variables, all fields are then interpolated onto a common grid at the coarsest resolution (i.e., 1° resolution) within the diagnostic domain. After removing extreme outliers (∼99th percentile), each variable is normalised by its basin-wide maximum to ensure equal weighting. The SOM algorithm is then applied to the normalised seasonal cycles and generates 3,522 initial clusters. These clusters are subsequently merged into broader groups using the unsupervised HAC algorithm. At the level of five clusters, the four target regimes are recovered, with the subtropical regime remaining represented by two clusters that share a common oligotrophic gyre signature but differ in their seasonality and degree of stratification. Given their broad similarity relative to the other regimes, these two clusters are subsequently combined into a single bioregion for analysis, resulting in a final set of four bioregions of the obervations (bioregion boundaries indicated by dashed lines in Fig. 1a,d).

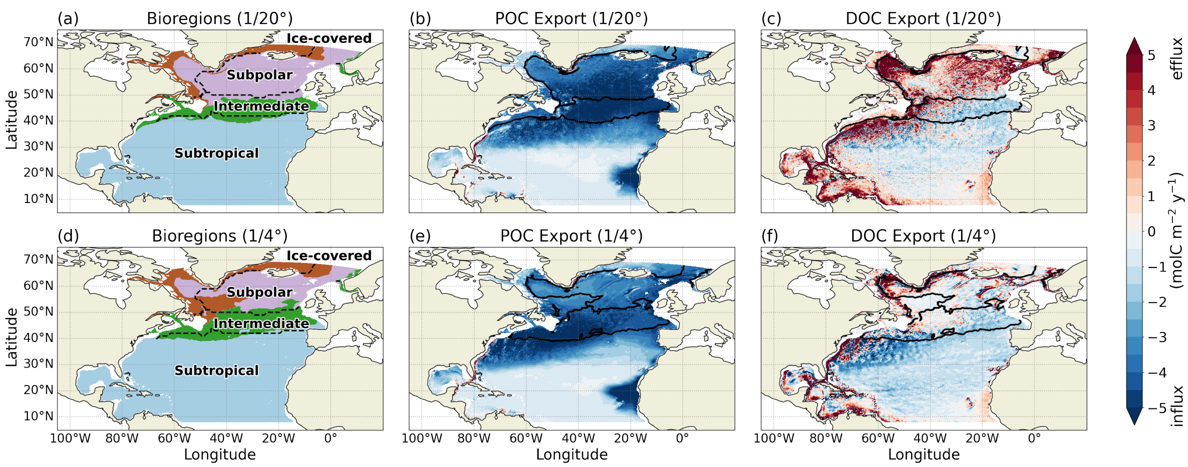

Figure 1. Bioregions determined using the SOM + HAC procedure and organic carbon export at the base of the mixed layer in the $1/20°$ and $1/4°$ simulations. The top row (a–c) corresponds to the $1/20°$ simulation and the bottom row (d–f) to the $1/4°$ simulation. (a, d) Bioregions, with colours indicating the different regions and dashed lines marking bioregion boundaries derived from observations (cf. Table A1). (b, e) Annually averaged POC export flux and (c, f) annually averaged DOC export flux at the base of the mixed layer. Exports are expressed in $\mathrm{molC\,m^{-2}\,yr^{-1}}$; positive values indicate efflux of organic carbon from the ocean interior to the mixed layer and negative values indicate influx to the ocean interior. Solid lines in the export maps indicate the bioregion boundaries of the corresponding simulation.

Bioregions in the simulations are also constructed by applying the SOM + HAC procedure to the outlier-filtered, normalised climatological seasonal cycles of the same five variables in the simulations, but with each grid cell assigned to the nearest observational initial clusters. Using the same initial clusters ensures a consistent cluster framework across the observational and simulated datasets, while still allowing the clusters to represent the characteristic conditions in the model simulations. The resulting bioregions obtained in the simulations are broadly consistent with those inferred from observations, featuring a

https://doi.org/10.5194/egusphere-2026-4891
Preprint. Discussion started: 28 September 2026

larger subtropical region and smaller regions elsewhere (bioregions indicated by colours in Fig. 1a,d). Differences among the three estimates increase toward higher latitudes in the subpolar and ice-covered regions, consistent with model limitations in resolving high-latitude processes (Hallberg, 2013).

2.3 Subduction and sedimentation exports

The calculation of subduction and sedimentation exports follows the framework of Lévy et al. (2013), in which the export is defined as the net flux of tracers across the base of the seasonally varying mixed layer, while biologically mediated transfer is not represented (see their Fig. 1 and Eq. (2)). These fluxes are computed online at each model time step. To recap, the tracer evolution equation is vertically integrated from the surface to the mixed-layer base of height h, resulting in

$$h\,\partial_t C_h = \underbrace{-C_h\,\mathbf{u}_h\cdot\nabla_H h - C_h\,w_h + \int_0^h E_C\,dz}_{\text{Advective export}} + \underbrace{(k_z\,\partial_z C)_h - C_h\,\partial_t h}_{\text{Mixed-layer export}} + \underbrace{\int_0^h S_C^{sink}\,dz}_{\text{Sedimentation export}} + \underbrace{\int_0^h S_C^{other}\,dz}_{\text{Others}}, \qquad (1)$$

where C is tracer concentration, and C_h is concentration at the base of the mixed layer. The term $h\,\partial_t C_h$ on the left represents the rate of change of tracer content inside a mixed-layer volume, assuming a vertically uniform tracer concentration within that volume. On the right-hand side of the equation, the terms $C_h\,\mathbf{u}_h\cdot\nabla_H h$ and $C_h\,w_h$ represent the tracer fluxes at the base of the mixed layer due to lateral advection and vertical advection, respectively, while $\int_0^h E_C\,dz$ denotes the contribution from lateral eddy-induced diffusion; together these three fluxes constitute the advective export. The vertical diffusive flux $(k_z\,\partial_z C)_h$, together with the entrainment term $C_h\,\partial_t h$ associated with deepening or shoaling of the mixed layer, composes the mixed-layer export. The term $\int_0^h S_C^{sink}\,dz$ represents sedimentation export. Other biological sources and sinks within the mixed layer are collected in $\int_0^h S_C^{other}\,dz$. Note that in this equation, when C represents DOC, the sedimentation term vanishes and each term describes the direct action of processes on DOC. When C represents POC, it is not described by a single tracer in the model; instead, it is defined as the sum of phytoplankton (nanophytoplankton and diatoms), zooplankton (micro- and mesozooplankton), and sinking particles (small and large size classes). Consequently, each term in the equation is calculated as the combined contribution of the these individual components, and the sedimentation term represents the sinking of both classes of sinking particles.

The resulting vertically integrated tendencies are examined over the North Atlantic basin and the defined bioregions using spatially integrated exports to characterise the overall magnitude of carbon export (Appendix B), while the analysis focuses primarily on export fluxes, which are independent of spatial extent and therefore allow more robust comparisons of export intensity across bioregions (cf. Fig. 1). Annually averaged budgets are obtained by averaging the online tendencies over the five-year diagnostic period, while seasonal variability is characterised using monthly climatologies computed over the same period (i.e., from the start of 1974 to the end of 1978).

https://doi.org/10.5194/egusphere-2026-4891
Preprint. Discussion started: 28 September 2026

3 Results

3.1 Annually averaged organic carbon export

The spatially integrated POC export in the North Atlantic basin amounts to $1.19\,\mathrm{PgC\,yr^{-1}}$ (cf. Fig. B1a) and is dominated by sedimentation export, while subduction export contributes $30\,\%$ of the total, with advective and mixed-layer export accounting for $19\,\%$ and $11\,\%$, respectively (Fig. 2c), corresponding to an ∼2:1 ratio. The dominance of sedimentation export, being by definition restricted to influx, is reflected in the spatial prevalence of influx (Fig. 1b). This partitioning is broadly consistent across bioregions, with sedimentation export dominating, subduction export contributing 22–34$\,\%$, and advective and mixed-

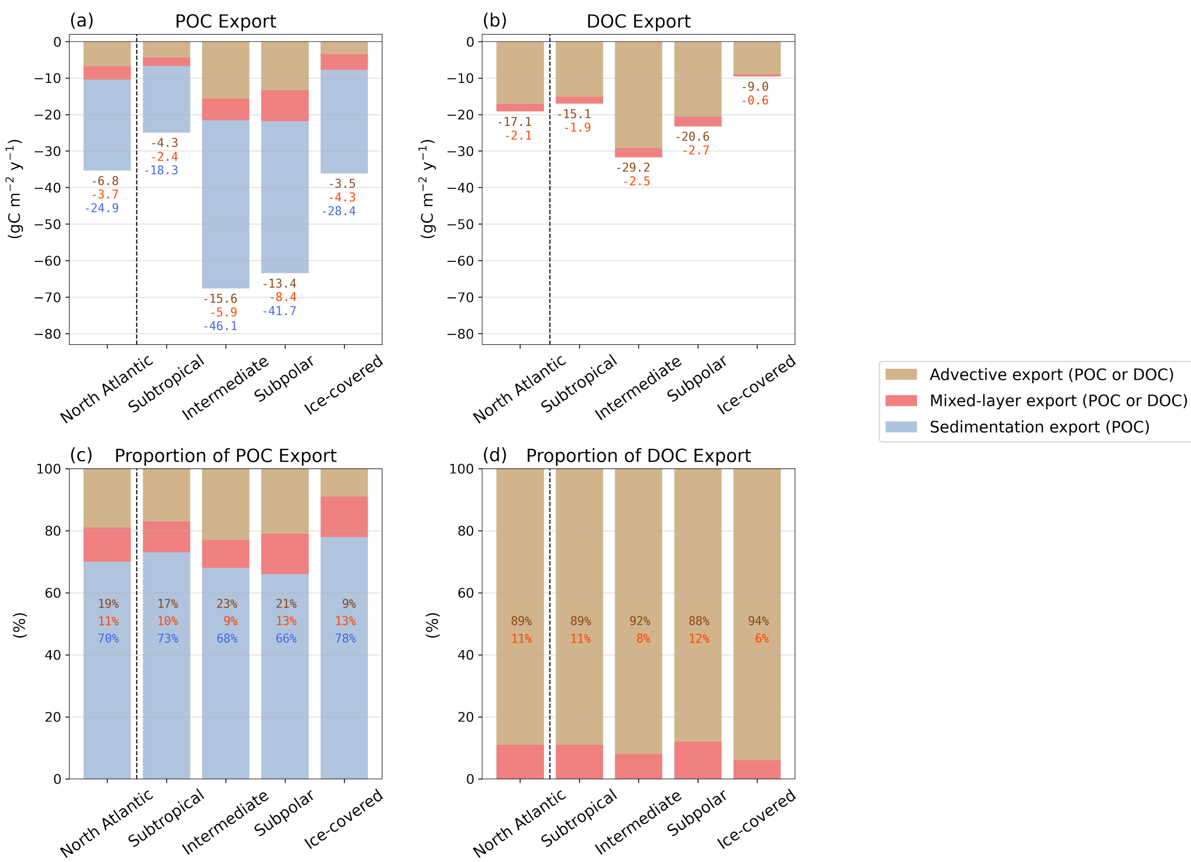

Figure 2. Annually averaged organic carbon export flux in the $1/20^{\circ}$ simulation for the North Atlantic and each bioregion, decomposed into advective export (brown), mixed-layer export (red), and sedimentation export (blue). (a, b) Export flux of POC and DOC at the mixed-layer base ($\mathrm{gC\,m^{-2}\,yr^{-1}}$); negative values indicate influx of organic carbon from the mixed layer to the ocean interior. (c, d) Proportion of each export pathway for POC and DOC export flux (%). Numerical values are shown in the corresponding colours. Note that DOC has no sedimentation export by definition.

https://doi.org/10.5194/egusphere-2026-4891
Preprint. Discussion started: 28 September 2026

layer export maintaining an ∼2:1 ratio except in the ice-covered region (Fig. 2c). Although the partitioning remains broadly consistent across bioregions, export intensity exhibits pronounced spatial contrasts (Fig. 2a). The total POC export flux is relatively low in the subtropical region, reaches a maximum in the intermediate region, and then decreases toward higher latitudes. The weak export in the subtropical region is consistent with its oligotrophic conditions (cf. Fig. A1e1). The maximum export in the intermediate region arises from strong sedimentation and advective contributions, which together offset the higher mixed-layer export in the subpolar region and result in a lower total export there. This enhanced export in the intermediate and subpolar regions is physically consistent with the circulation characteristics reported for the eddy-rich simulation on which the present simulation is based, including enhanced mesoscale variability in the western boundary currents and pronounced mixed-layer variability in the subpolar North Atlantic, which together favour more active physical transport than in the subtropical gyre (Biastoch et al., 2021). Farther north, all export components decline in the ice-covered region, where the physical conditions are relatively more stable, and the advective contribution is no longer larger than the mixed-layer component.

The spatially integrated DOC export in the basin scale is $0.65\,\mathrm{PgC\,yr^{-1}}$ (cf. Fig. B1c) and is dominated by advective export, which accounts for $89\,\%$ (Fig. 2d). This net DOC export reflects the compensation of localised efflux hotspots from the ocean interior to the mixed layer by influx elsewhere (Fig. 1c). The large contribution of advective export remains consistent across bioregions, at 88–$94\,\%$. This fraction is larger than that in POC subduction export, while advective export remains the dominant component of both DOC and POC subduction export. The intensity of DOC subduction export exceeds that of POC subduction export (Fig. 2a,b), though the DOC pool is not fully represented in the model (cf. Sect. 2.1). The regional distribution of DOC mirrors that of POC: total export flux is relatively low in the subtropical region, highest in the intermediate region, and gradually decreases toward higher latitudes.

3.2 Monthly variation in organic carbon export

The monthly variation of spatially integrated POC export in the North Atlantic basin shows that the peak in advective export during winter precedes the peak in mixed-layer export in spring, followed by the maximum of sedimentation export in late spring (Fig. 3a). The seasonal evolution of DOC export mirrors that of POC, with the peaks of the corresponding components occurring at similar times, such that advective export peaks before mixed-layer export. Together, these variations produce a peak in subduction export that precedes the peak in sedimentation export, indicating that subduction export together with sedimentation export plays a first-order role in shaping the seasonal variability of carbon export. Meanwhile, mixed-layer export becomes positive for both POC and DOC in late summer and beyond, reflecting an efflux from the ocean interior back to the surface layer. This strong seasonal variability leads to substantial cancellation between periods of influx and efflux, resulting in a relatively small annually averaged mixed-layer export and leaving advective export as the dominant component of subduction export for both POC and DOC (cf. Fig. 2).

Across bioregions, the timing of export peaks of both tracers broadly follows the basin-scale pattern: a winter–spring peak in advective export precedes the spring peak in mixed-layer export, followed by a spring–summer maximum in sedimentation export, although this sequence is less pronounced in the subtropical and ice-covered regions (Fig. 3b–e). An efflux associated with mixed-layer export that develops in late summer and persists thereafter, while being balanced by stronger influx during

https://doi.org/10.5194/egusphere-2026-4891
Preprint. Discussion started: 28 September 2026

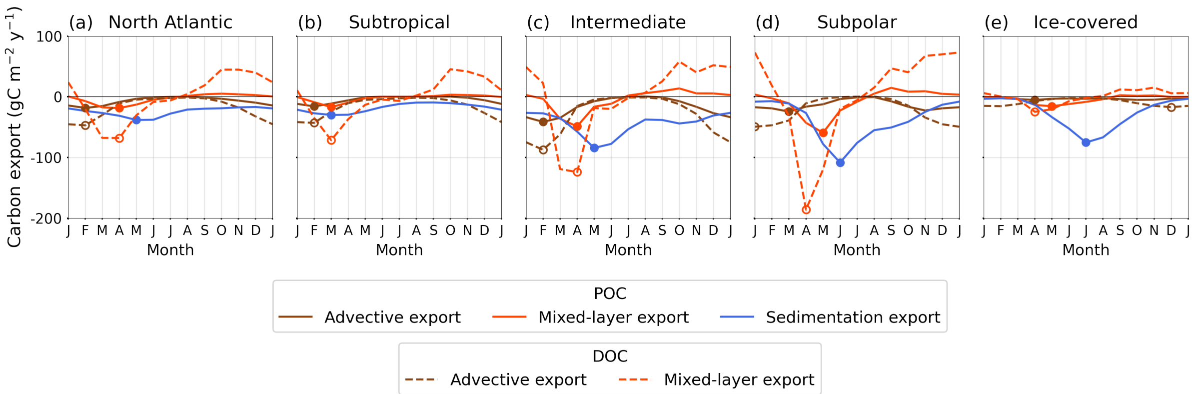

Figure 3. Monthly variation of organic carbon export flux in the $1/20°$ simulation for the North Atlantic and each bioregion, decomposed into advective export (brown), mixed-layer export (red), and sedimentation export (blue) for (a) the North Atlantic and bioregions of the (b) subtropical, (c) intermediate, (d) subpolar, and (e) ice-covered regions. POC export flux (solid lines) and DOC export flux (dashed lines) are both shown with their corresponding export pathways. Circle markers indicate the monthly peak of each pathway (solid markers for POC; hollow markers for DOC). All values are in $\mathrm{gC\,m^{-2}\,yr^{-1}}$; positive values indicate efflux of organic carbon from the ocean interior to the mixed layer and negative values indicate influx to the ocean interior. Note that DOC has no sedimentation export by definition.

the remaining seasons, is also observed across bioregions. Beyond the consistent timing, the magnitude of seasonal variability exhibits a distinct spatial pattern, being lower in the subtropical region, increasing in the intermediate and subpolar regions, and then decreasing toward the ice-covered region. This spatial structure corresponds closely to the pattern in annually averaged export (cf. Fig. 2a,b). In the subtropical region, the lower variability is consistent with its lower annually averaged export. Relative to the subpolar region, the intermediate region shows a lower variability in mixed-layer and sedimentation exports and a higher variability in the advective export; together, this results in a higher annually averaged total export of both tracers. In the ice-covered region, the variability is high in the sedimentation export but remains minor in the advective and mixed-layer components, consistent with the relatively stable conditions there.

3.3 Variability in annual organic carbon export: eddy-rich vs. eddy-present simulations

The spatially integrated POC export in the North Atlantic basin is $1.07\,\mathrm{PgC\,yr^{-1}}$ in the eddy-present $1/4°$ simulation, with the eddy-rich $1/20°$ simulation exhibiting an export that is higher by $11\,\%$ relative to $1/20°$ (Fig. 4a; cf. Fig. B1b). This greater export is driven by a substantial increase in advective export ($+49\,\%$) and a modest increase in sedimentation export ($+6\,\%$), partly offset by a small decrease in mixed-layer export ($-23\,\%$). This difference coincides with previously reported differences in the physical circulation between model simulations similar to those used here, whose distinct circulation patterns provide different physical environments for organic carbon export (Biastoch et al., 2021). At the regional scale, POC export intensity is higher across all bioregions except the ice-covered region, with the larger differences observed at mid-to-high latitudes (values in grey in Fig. 4a), reaching up to $26\,\%$ in the subpolar region. In the subtropical, intermediate, and subpolar regions, the higher

https://doi.org/10.5194/egusphere-2026-4891
Preprint. Discussion started: 28 September 2026

total export fluxes are likewise associated with enhanced advective and sedimentation exports combined with reduced mixed-layer export. The increase in advective export generally exceeds that in sedimentation export, suggesting that the advective component of POC export is particularly sensitive to model resolution. This sensitivity likely arises because higher resolution enhances small-scale variability, which can also modify large-scale fluxes; this issue will be revisited in the discussion section. This highlights the importance of adequately representing ocean dynamics in ocean models to better constrain physically driven subduction export. For the difference in mixed-layer export, this likewise coincides with previously reported differences in mixed-layer structure and deep convection dynamics, whereby the eddy-rich simulation resolves mesoscale eddy influences on the spatial structure of deep convection that are not represented in the eddy-present simulation (Biastoch et al., 2021). In contrast, the ice-covered region exhibits a decrease in total POC export with a decrease in sedimentation export. This overall decrease in POC export is consistent with a larger sea-ice fraction, which promotes more stable upper-ocean conditions (cf. the last column in Fig. A1).

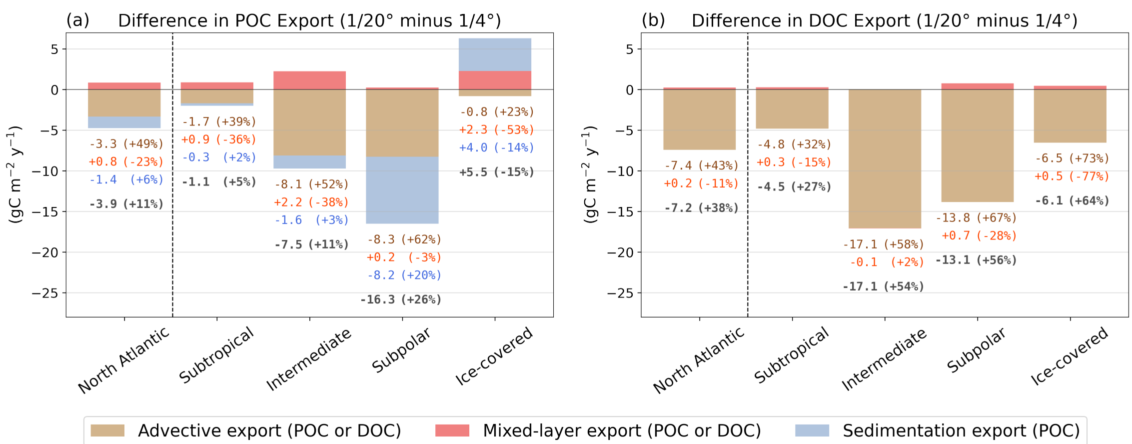

Figure 4. Difference in annually averaged organic carbon export flux between the $1/20^{\circ}$ (cf. Fig. 2) and $1/4^{\circ}$ simulations ($1/20^{\circ}$ minus $1/4^{\circ}$) for the North Atlantic and each bioregion, decomposed into advective export (brown), mixed-layer export (red), and sedimentation export (blue). (a) Differences in POC export and (b) differences in DOC export at the mixed-layer base. Numerical values ($\mathrm{gC\,m^{-2}\,yr^{-1}}$) and percentage changes (%; in brackets) relative to the raw values in $1/20^{\circ}$ are shown in the corresponding colours, and the grey values indicate the total change in the North Atlantic and each bioregion. Positive values and negative percentages indicate a smaller influx of organic carbon from the mixed layer to the ocean interior in the $1/20^{\circ}$ simulation, whereas negative values and positive percentages indicate a larger influx. Note that DOC has no sedimentation export by definition.

The basin-scale integrated DOC export accounts for $0.41\,\mathrm{PgC\,yr^{-1}}$ in the $1/4^{\circ}$ simulation and is $38\,\%$ higher in $1/20^{\circ}$ (Fig. 4b; cf. Fig. B1d). This increase largely arises from increased advective export ($+43\,\%$), alongside a small decrease in mixed-layer export ($-11\,\%$). Export intensity increases across all bioregions, with the largest changes, as for POC, occurring at mid-to-high latitudes. The intermediate region exhibits the largest absolute increase in total DOC export, while the ice-covered region shows the greatest relative increase, reaching up to $64\,\%$. The regional patterns of each pathway mirror the

https://doi.org/10.5194/egusphere-2026-4891
Preprint. Discussion started: 28 September 2026

basin-scale response, with higher advective export and lower mixed-layer export, again similar to POC. An exception occurs in the intermediate region, where mixed-layer export is slightly higher, although this contribution remains minor. The pronounced differences in advective DOC export among bioregions also highlight the sensitivity of the advective component to model resolution.

4 Discussion

4.1 How do our findings extend previous understanding?

Several previous modelling studies have also examined the physically driven subduction export of organic carbon. In a global ocean model, Lévy et al. (2013) evaluated global-scale organic and inorganic carbon fluxes across the mixed layer and introduced a diagnostic framework that we adopt here. The nominal model resolution of $2°$ used in that study is insufficient to resolve mesoscale features (Hewitt et al., 2017, 2022), which are essential to shape mixed-layer dynamics and carbon export (see the following subsection). Nevertheless, our results reproduce a similar spatial pattern of combined POC and DOC subduction export in the North Atlantic, with the maximum export occurring near western boundary current regions (cf. Fig. 1b,c,e,f, and their Fig. 4b,d). However, the magnitude of the subduction export differs substantially. While mixed-layer export is comparable between the two studies with $\sim 0.2\,\mathrm{PgC\,yr^{-1}}$, advective export is larger in our simulations with 0.8 and $0.4\,\mathrm{PgC\,yr^{-1}}$ in the $1/20°$ and $1/4°$ simulations, respectively, compared with $\sim 0.1\,\mathrm{PgC\,yr^{-1}}$ reported in their study (cf. Fig. B1, and their Fig. 3c). This difference further implies that advective export is particularly sensitive to model resolution (cf. Sect. 3.3), and its increase with resolution may reflect differences in how advection and eddy-induced diffusion are represented, although differences in domain definition between the studies may contribute. This underscores the need to incorporate resolution-dependent physical dynamics into biogeochemical models to more accurately represent export pathways.

A complementary perspective is provided by Resplandy et al. (2019), who used an idealised North Atlantic configuration at $1/54°$. Although the idealised nature of their configuration and the use of a different diagnostic framework precludes direct quantitative comparison with our results, their findings suggest that eddy subduction pump represents a relatively small net contribution to annual organic carbon flux at the basin-scale ($< 5\,\%$) due to strong compensation between upward and downward motions (cf. their Fig. 4b,d). This is despite the relatively high probability of POC eddy downward subduction in the North Atlantic compared to other regions of the global ocean, inferred from a detection algorithm applied to observations (Keutgen De Greef et al., 2026). Our investigation extends these previous efforts by employing eddying models in a more realistic framework to examine organic carbon export, while also evaluating its sensitivity to model resolution under different representations of eddying processes. Note that in the present study, the eddy subduction pump is embedded within the advective export (cf. Eq. (1)), which in both simulations consists of contributions from eddy-induced advection that is partially resolved explicitly and eddy-induced diffusion parameterised along isoneutral directions (Redi 1982; cf. Table 1). This differs from previous frameworks that isolate the eddy component as a separate eddy subduction pump, as well as from observational studies that typically consider only downward eddy subduction by instead quantifying net subduction as the balance of influx and efflux across multiple spatial dimensions at the mixed-layer base (Boyd et al., 2019).

https://doi.org/10.5194/egusphere-2026-4891
Preprint. Discussion started: 28 September 2026

Using the same biogeochemical model and an identical diagnostic framework implemented with the same code, Le Chevère et al. (2026) conducted a similar analysis for the Southern Ocean using a global ocean model at $1/4°$ resolution. Despite focusing on a different basin, both studies identify sedimentation export as the dominant pathway of total organic carbon export, while subduction export remains an important pathway (cf. Fig. 2 and Fig. B1; their Fig. 6). The sequence of monthly peaks among the export pathways of both tracers is likewise evident in the Southern Ocean, with each pathway reaching its maximum during the seasons corresponding to that observed in the North Atlantic (cf. Fig. 3, and their Fig. S9). This consistency reinforces our conclusion that, alongside the gravitational pump, subduction export plays an important role in determining the seasonal timing of total organic carbon export, with important implications for the design of future ocean observing systems. Nevertheless, differences remain between the results of the two studies, reflecting the distinct characteristics of the North Atlantic and Southern Ocean.

4.2 What are the main uncertainties of this study?

A key limitation of the model configuration concerns the representation of DOC, which is treated solely as a semi-labile pool while neglecting the labile and refractory components. This simplification leads to a bias in DOC export because the absence of a labile pool removes any potential short-lived contribution to export, particularly in the eddy-rich simulation where eddy subduction pump can inject this transient component below the mixed layer, and the absence of a refractory pool neglects the fraction of exported carbon that is transferred into long-lived storage (Hansell, 2013; Hansell and Orellana, 2021). While the semi-labile pool captures the dominant DOC fraction that accumulates and is transported across the mixed-layer base, the results may still be regarded as a reasonable first-order estimate of DOC export. However, this simplification also limits model evaluation against observations, as it prevents a direct comparison with the full observed spectrum of DOC lability (cf. row g in Fig. A1).

In addition, the diagnostic framework introduces uncertainties through its definition of the reference surface based on the time-varying mixed-layer depth (cf. Eq. (1)) rather than a fixed depth (e.g., $100\,\mathrm{m}$; Resplandy et al., 2019; Palevsky and Doney, 2021). This choice provides a dynamically consistent measure of carbon export across the evolving interface between the surface layer influenced by the atmosphere and the ocean interior. However, the resulting estimates are sensitive to the simulated mixed-layer variability and limit direct comparison with export diagnostics defined at fixed reference depths, since changes in mixed-layer depth can modify the position of the reference surface independently of changes in the underlying carbon export processes.

A further source of uncertainty arises from the bioregion construction through the SOM + HAC procedure. Relative to fixed biogeographic regionalisations (e.g., Longhurst code: Longhurst, 2010), this procedure yields regions that are more internally coherent with respect to the simulated physical and biogeochemical structure. Consequently, when the two simulations are compared using their own tailored bioregions (cf. Fig. 4), variation in organic carbon export arises from both differences in intrinsic variation in export behaviour and basin-scale physical and biological conditions that shape the emergent bioregions. A complementary experiment, in which the variability between the two simulations (cf. Sect. 3.3) is restricted to organic carbon export using the same biogeographical areas as defined by the bioregions in $1/20°$ (cf. Fig. 1a) for both simulations, shows

https://doi.org/10.5194/egusphere-2026-4891
Preprint. Discussion started: 28 September 2026

slight differences while leaving the main conclusions unchanged (Appendix C). This suggests that the simulated variability arises primarily from intrinsic differences in export behavior, rather than from differences in the bioregions. This may partly reflect the fact that the bioregions are constructed from variables relevant to the physical and biological behaviours while excluding the export metric itself, thereby weakening any direct coupling between the regionalisation and the simulated export field and preserving an independent basis for evaluating export across bioregions. Overall, the bioregions are not unique, as their boundaries depend on methodological choices including the selected variables, the number of clusters, and the clustering algorithm (alternative algorithms such as k-means, following McQueen, 1967 and Lloyd, 1982, and Gaussian mixture models, following Reynolds, 2015).

Even at the eddy-present to eddy-rich resolutions employed in this study, eddy processes across scales remain only partially resolved, introducing biases in the diagnosed organic carbon export. Locally, small-scale frontal features can generate intense eddy subduction (Lévy et al., 2012a), which has been suggested to contribute substantially to the springtime export of small nonsinking POC (Omand et al., 2015). Beyond their direct subduction effects, remote eddy effects on overturning circulation (Lévy et al., 2010; Marshall et al., 2017; Mak et al., 2018; Hewitt et al., 2020; Fortin et al., 2023), mixed-layer depth (Lévy et al., 2012b; Amores et al., 2017; Treguier et al., 2023), and nutrient availability (Lévy et al., 2001; Lévy, 2003; Mahadevan, 2016; Couespel et al., 2021; Lévy et al., 2024; Ruan et al., 2023, 2024) can also regulate primary production and export processes. The previous study using simulations comparable to those employed here shows that the eddy-rich simulation, compared with the eddy-present simulation, exhibits substantially stronger mesoscale variability, more realistic Gulf Stream separation and North Atlantic Current pathways, a stronger and deeper Atlantic Meridional Overturning Circulation, and more realistic overflow and deep-convection structures associated with resolved mesoscale eddies (Biastoch et al., 2021), which together can alter the physical pathways. However, reliance on eddy closures may further compound the uncertainty: conventional Gent-McWilliams parameterisations are designed for non-eddying resolution (Gent et al., 1995), and although recent developments such as the backscatter approach (Jansen et al., 2015a, b; Bachman, 2019) and the splitting approach (Mak et al., 2023) provide frameworks to adjust eddy-induced transport at eddy-permitting resolution, these schemes are not yet widely implemented. The present study does not employ these aforementioned parameterisations and provides only a relatively more reliable estimate of organic carbon export compared to using coarser-resolution models. Consequently, the resolution-dependent differences identified here should be interpreted more broadly as arising from the enhanced representation of ocean physics and transport processes in the $1/20°$ simulation relative to the $1/4°$ simulation, independent of the eddy parameterisations considered above. Further refinement of organic carbon export estimates will require either more robust eddy parameterisations or higher model resolution capable of explicitly resolving eddy dynamics, particularly for the advective export component and at mid-to-high latitudes in the North Atlantic, both of which exhibit more sensitivity to model resolution.

https://doi.org/10.5194/egusphere-2026-4891
Preprint. Discussion started: 28 September 2026

5 Conclusions

Using a realistic eddy-rich model configuration, this study provides a quantitative assessment of the role of physically driven subduction export in North Atlantic POC and DOC export. The diagnostics establish a regional and seasonal context for export variability, complemented by a comparison with an eddy-present configuration, to address the three central questions that motivate the results presented below.

First, annually averaged export shows that subduction export contributes up to 34% of total POC export across bioregions, while sedimentation export remains the dominant pathway; the subduction component is partitioned between advective and mixed-layer export in an $\sim$2:1 ratio except in the ice-covered region. DOC export is similarly dominated by the advective component within subduction, accounting for up to 94% across bioregions. This partitioning in both tracers is broadly consistent across bioregions, despite the presence of coherent spatial patterns in total export flux for the tracers: lower export in the oligotrophic subtropical region, a maximum in the intermediate region, and a decline toward the subpolar and ice-covered regions.

Second, the seasonal variation of the export pathways is broadly consistent across tracers and bioregions: winter–spring advective export precedes the spring peak in mixed-layer export, followed by enhanced sedimentation in spring–summer. This sequence highlights the important role of subduction export, together with sedimentation export, in governing the seasonal evolution of organic carbon export. Meanwhile, mixed-layer processes drive an efflux of organic carbon from late summer onward, but influx dominates on the annual scale.

Third, comparison with the eddy-present simulation reveals a pronounced sensitivity of organic carbon export to model resolution: export is higher in the eddy-rich simulation for both tracers across most bioregions, with differences largest at mid-to-high latitudes and reaching up to 26% for POC in the subpolar region and 64% for DOC in the ice-covered region. The advective component shows particular sensitivity to model resolution, highlighting the importance of accurately representing the processes governing physically driven subduction export.

Overall, these results demonstrate that physically driven subduction export of organic carbon in the North Atlantic exhibits pronounced regional and seasonal variability and strong sensitivity to model resolution. These findings place additional constraints on physically driven subduction export in the North Atlantic and refine our understanding of its role in ocean carbon cycling. They further highlight the need for improved constraints on subduction export from both observational and modelling perspectives.

https://doi.org/10.5194/egusphere-2026-4891
Preprint. Discussion started: 28 September 2026

Code and data availability. The data and code necessary to reproduce the findings of this study will be made publicly available upon publication. A preliminary repository record and associated DOI can be provided to reviewers upon request during the peer-review process.

Appendix A: Model evaluation

The performance of the ORCA025.L46-KFS006-P-V ($1/4°$) and VIKING20X.L46-KFS007-Pa ($1/20°$) simulations (cf. Sect. 2.1) is evaluated here with a focus on the variables that are most relevant to constrain organic carbon export. Both of their configurations have been widely applied in previous studies and the present analysis provides an extension for their assessment. The observational datasets used for the evaluation are summarised in Table A1, including the five variables employed for bioregion construction, specifically sea surface temperature (SST), sea-ice area fraction (ICE), mixed-layer depth (MLD), surface nitrate concentration (NO3), surface chlorophyll concentration (CHL), in addition to surface POC and DOC concentrations. The datasets are selected to permit meaningful comparison with the simulations. Consistent with the data treatment used for

	Spatial resolution	Temporal resolution	Coverage	Data Source and reference
Sea surface temperature (SST, $°C$)	$1/2°$	Monthly	Jan 1960 – Jun 2024 Global	Copernicus Marine Service (ID: INSITU_GLO_PHY_TS_OA_MY_013_052) Szekely et al. (2019)
Sea-ice area fraction (ICE)	$1/4°$	Daily (every other day in pre-Jul 1987), monthly	Nov 1978 – Dec 2024 Polar regions	National Snow and Ice Data Center (ID: NSIDC-0079) Comiso (2017)
Mixed-layer depth (MLD, m)	$1°$	Monthly climatology	1970 – 2021 Global	Mixed layer depth over the global ocean (LOPS, IFREMER) de Boyer Montégut (2024)
Nitrate (NO3, $\mu mol\,kg^{-1}$)	$1°$	Monthly climatology	1965 – 2022 Global	World Ocean Atlas 2023 (WOA23) Reagan et al. (2023)
Chlorophyll (CHL, $mgC\,m^{-3}$)	$1/4°$	Monthly	Jan 1998 – Dec 2022 Global	Copernicus Marine Service (ID: MULTIOBS_GLO_BIO_BGC_3D_REP_015_010)
Particular organic carbon (POC, $mgC\,m^{-3}$)				
Dissolved organic carbon (DOC, $\mu molC\,kg^{-1}$)	$9\,km$	Monthly	Jan 2010 – Dec 2018 Global	BICEP : Monthly global dissolved organic carbon (DOC) Laine et al. (2024)

Table A1. Observational datasets. Listed are the key variables, spatial resolutions, temporal resolutions, coverage, data sources and references. Variables include sea surface temperature (SST, $°C$), sea-ice area fraction (ICE), mixed-layer depth (MLD, m), surface nitrate concentration (NO3, $\mu mol\,kg^{-1}$), surface chlorophyll concentration (CHL, $mgC\,m^{-3}$), surface particulate organic carbon concentration (POC, $mgC\,m^{-3}$), and surface dissolved organic carbon concentration (DOC, $\mu molC\,kg^{-1}$).

https://doi.org/10.5194/egusphere-2026-4891
Preprint. Discussion started: 28 September 2026

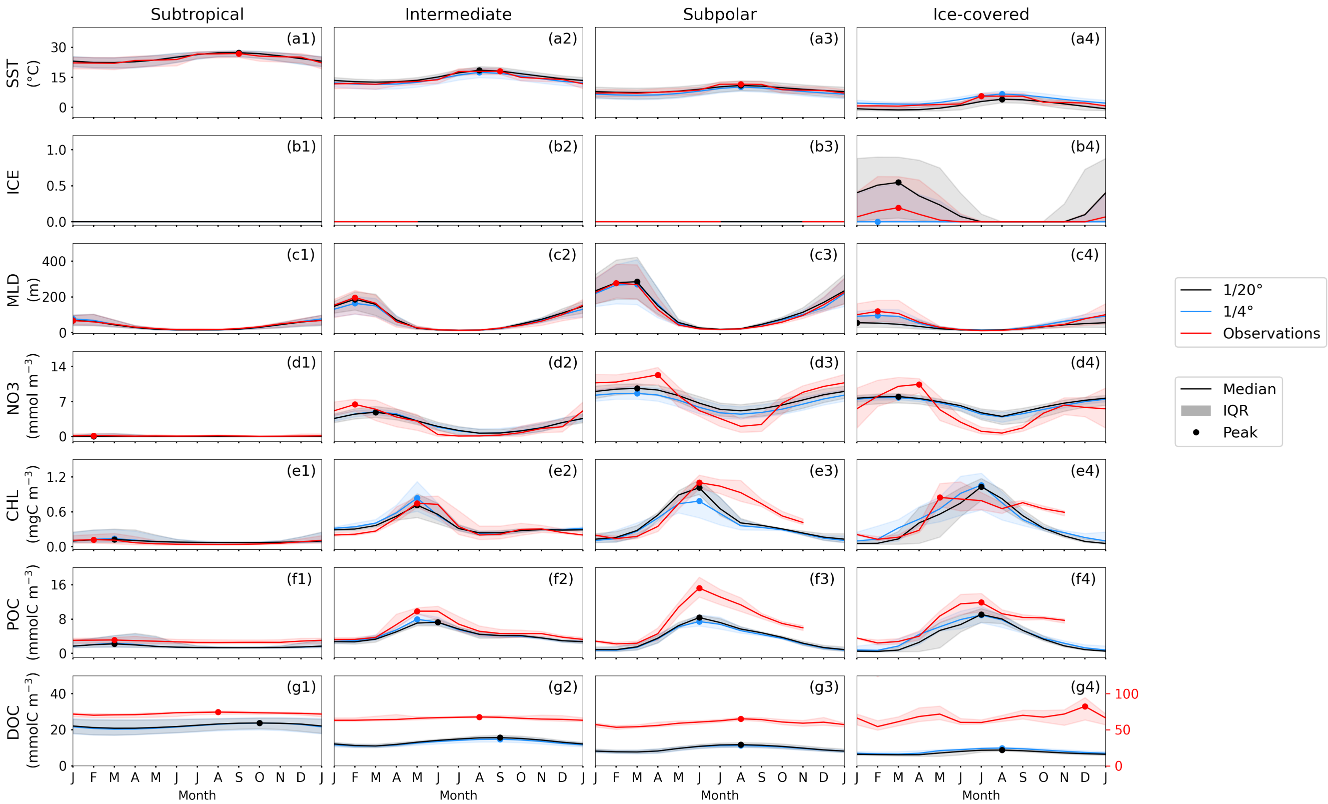

Figure A1. Monthly variation of key variables from the $1/4°$ simulation (blue), $1/20°$ simulation (black), and observations (red), showing the median (solid lines), interquartile range (IQR; shading), and annual peak (solid markers). Rows show a) sea surface temperature (SST, $°C$), (b) sea-ice area fraction (ICE), (c) mixed-layer depth (MLD, m), (d) surface nitrate concentration (NO3, $mmol\,m^{-3}$), (e) surface chlorophyll concentration (CHL, $mgC\,m^{-3}$), (f) surface particulate organic carbon concentration (POC, $mmolC\,m^{-3}$), and (g) surface dissolved organic carbon concentration (DOC, $mmolC\,m^{-3}$). Columns show the (1) subtropical, (2) intermediate, (3) subpolar, and (4) ice-covered regions. Note that for DOC, simulated values are smaller than those from observations and they are plotted using different y axis scales. Observational coverage for some variables is incomplete in space and time, and values are therefore based on available observations only.

bioregion construction, all fields are interpolated onto a $1°$ grid within the diagnostic domain and averaged across years to obtain monthly values following the same temporal coverage strategy. Seasonal cycles of the median and interquartile range (IQR) are used to provide a concise measure of central tendency and variability.

Both simulations broadly agree with the observed seasonal cycles (Fig. A1). For SST (panels in row a), both simulations capture warmer conditions in the south and colder conditions at higher latitudes, with seasonal maxima occurring in summer, generally consistent with the observed climatology. ICE (panels in row b) is confined to the northernmost region in both simulations and observation. Although the median differs between them, the wide IQR indicates high variability and substantial overlap. MLD (panels in row c) deepens in winter and early spring and is shallower in subtropical and ice-covered regions and

https://doi.org/10.5194/egusphere-2026-4891
Preprint. Discussion started: 28 September 2026

deeper elsewhere. NO3 (panels in row d) peaks align with MLD due to entrainment and declines later with biological uptake; however, the simulated seasonal range is weaker than observed, except in the subtropical region where it remains low year-round. The subsequent spring bloom is captured, with CHL (panels in row e) peaking shortly after the NO3 maximum. For POC (panels in row f), the seasonal maximum generally coincides with the timing of the CHL bloom, but the bias relative to observations in the subpolar region is relatively pronounced. Finally, the DOC is lower in the simulations than observed (panels in row g), because only the semi-labile pool is represented in the model, whereas observational estimates may reflect a broader range of components (cf. Sect. 2.1 and 4.2). In general, the simulation biases may affect the resulting export estimates, but some observational records extend beyond the simulation period and may include stronger climate change signals. The simulations are also evaluated using a common set of bioregions derived from the $1/20°$ simulation and applied consistently to the observations and both simulations, so as to isolate local model behaviour from differences arising from the bioregions. The results remain broadly similar (not shown), with only slightly larger differences in the ice-covered region, reflecting greater differences in the definition of that region among the cases (cf. Fig. 1a,d). Nevertheless, the broad agreement in the median and IQR of monthly diagnostics indicates that the simulations capture the dominant physical and biogeochemical controls relevant to the analysis.

Appendix B: Spatially integrated export

While the main text focuses on export fluxes ($\mathrm{gC\,m^{-2}\,yr^{-1}}$), which quantify the intensity of carbon export independently of bioregion area, Fig. B1 presents the corresponding spatially integrated export ($\mathrm{PgC\,yr^{-1}}$), reflecting both export intensity and spatial extent. Integrated POC and DOC exports broadly scale with the area of the bioregions, where in the $1/20°$ simulation the fractional area coverage from south to north is $73\,\%$, $9\,\%$, $15\,\%$, and $3\,\%$, and in the $1/4°$ simulation is $72\,\%$, $13\,\%$, $9\,\%$, and $6\,\%$, respectively. This suggests that spatial extent may contribute substantially to differences in integrated export, in addition to variations in export intensity. Accordingly, the main text uses area-normalised diagnostics to ensure that regional comparisons reflect intrinsic export strength rather than differences in area extent. More generally, comparisons between the simulations can be made using either export intensity or integrated exports, depending on whether the focus is on process-level differences or overall export from a region, with this study focusing on the former. Nevertheless, the relative contributions of the export components remain unchanged irrespective of the metric used (i.e., identical to those shown in Fig. 2c,d) for the $1/20°$ simulation.

Appendix C: Isolating export variability with fixed bioregions

To verify the conclusions regarding the variability of organic carbon export across model resolutions (see Sect. 3.3), the analysis is repeated using the same biogeographic localisation of bioregions in both simulations, thereby isolating variability due solely to export and excluding differences associated with the emergent bioregions. The biogeographical extend of the bioregions derived from $1/20°$ is adopted, as this simulation serves as the reference for assessing variability and yields bioregions

https://doi.org/10.5194/egusphere-2026-4891
Preprint. Discussion started: 28 September 2026

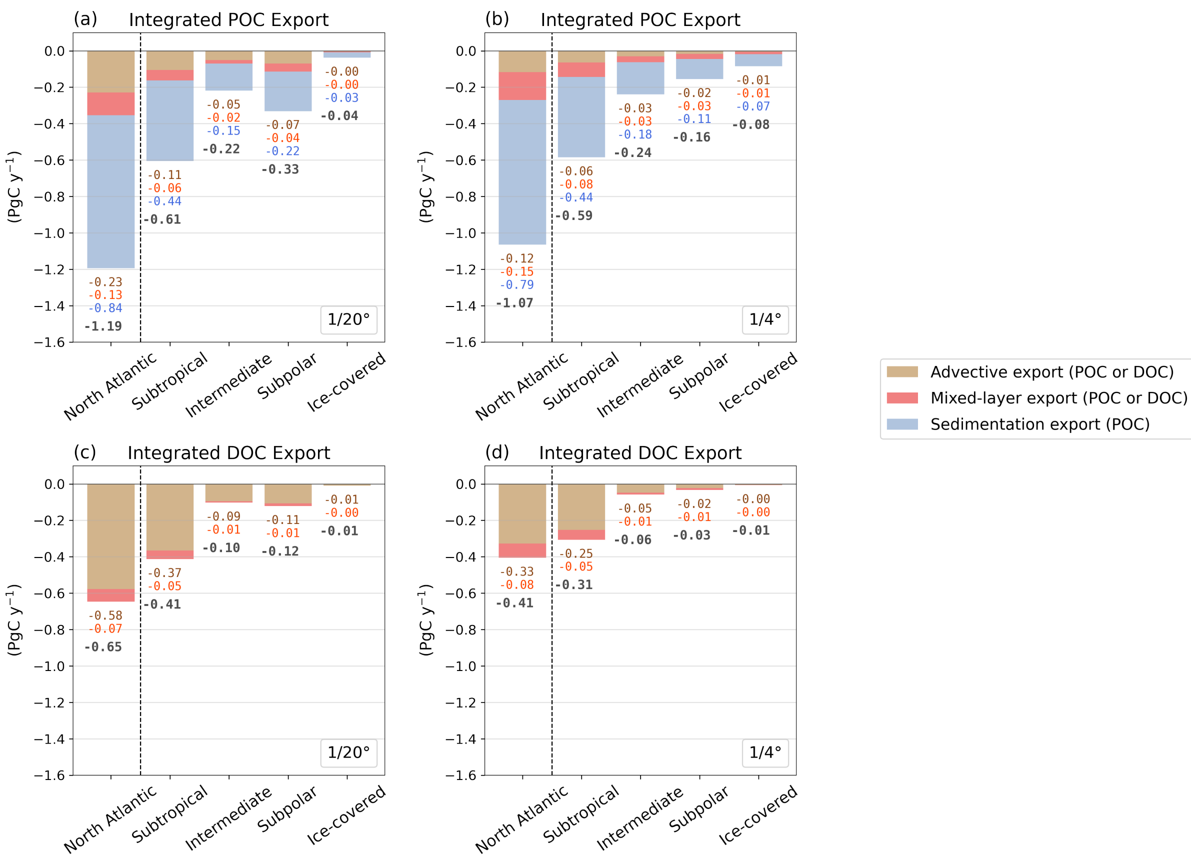

Figure B1. Similar as Fig. 2a,b, but showing the spatially integrated organic export ($\mathrm{PgC\,yr^{-1}}$) for the (a,c) $1/20°$ and (b,d) $1/4°$ simulations. The relative contributions of the export components are identical to those shown in Fig. 2c,d for the $1/20°$ simulation.

more consistent with that inferred from observations (cf. Fig. 1a,d; dashed lines indicates bioregion boundaries derived from observations). Using this common bioregional framework yields similar export variability between simulations to that obtained from their respective bioregional frameworks (transparent versus solid bars in Fig. C1). The main divergence at mid-to-high latitudes reflects the contrast between the $1/4°$ simulation analysed with its own emergent bioregions and the same simulation analysed using the reference set of bioregions. This likely arises from the larger mismatch in bioregional structure there, where the ice-covered region in $1/20°$ becomes smaller and no longer intrudes into the subpolar region. This stronger high-latitude discrepancies in variability and bioregion construction point to an enhanced sensitivity of physical and biological structure to model resolution in these regions, calling for caution in the interpretation of coarse-resolution simulations and underscoring the need for improved parameterisations of unresolved processes. Overall, the main conclusions remain unchanged, indicating that the simulated variability in export associated with model resolution reported in the main text arises primarily from intrinsic

https://doi.org/10.5194/egusphere-2026-4891
Preprint. Discussion started: 28 September 2026

differences in export behaviour rather than from differences in the bioregions themselves. Further evaluation using alternative sets of bioregions would also be valuable to assess the generality of this result.

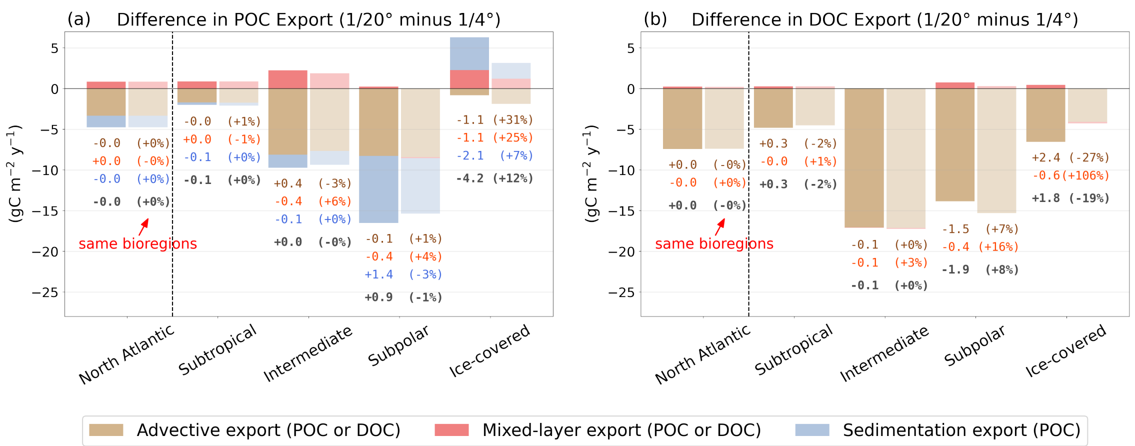

Figure C1. Same as Fig. 2, but also showing the difference in annually averaged organic carbon export flux between the $1/20°$ and $1/4°$ simulations when both are analysed using the same biogeographic localisation of bioregions derived from $1/20°$. Solid bars are the same as in Fig. 2 and correspond to the difference obtained with each simulation's own emergent bioregions; transparent bars show the difference obtained using the $1/20°$ bioregions. Numerical values ($\mathrm{gC\,m^{-2}\,yr^{-1}}$) and percentage changes (%; in brackets) relative to the raw values in $1/20°$ are the differences between each pair of bars, and indicate the effect of analysing the $1/4°$ simulation with its own emergent bioregions or with the $1/20°$ set of bioregions.

Author contributions. XR, SD, ML, and LB contributed to the conceptualisation of the study. XR and SD performed the formal analysis. FS and AB developed and implemented the modeling framework and generated the model outputs. ML, LB, and JM supervised the study. XR and SD wrote the original draft of the manuscript. All authors contributed to reviewing and editing the manuscript and approved the final version.

Competing interests. The authors declare that they have no conflict of interest.

https://doi.org/10.5194/egusphere-2026-4891
Preprint. Discussion started: 28 September 2026

Acknowledgements. XR, JM and ML were supported by a grant from the ANR/RGC Joint Research Scheme sponsored by the Research Grants Council of the Hong Kong Special Administrative Region, China and French National Research Agency (Project No. A-HKUST604/25). The authors gratefully acknowledge the Earth System Modelling Project (ESM) for funding this work by providing computing time on the ESM partition of the supercomputer JUWELS at the Jülich Supercomputing Centre (JSC).

References

Amores, A., Melnichenko, O., and Maximenko, N.: Coherent mesoscale eddies in the North Atlantic subtropical gyre: 3-D structure and transport with application to the salinity maximum, J. Geophys. Res. Oceans, 122, 23–41, https://doi.org/10.1002/2016JC012256, 2017.

von Appen, W.J., Waite, A.M., Bergmann, M., Bienhold, C., Boebel, O., Bracher, A., Cisewski, B., Hagemann, J., Hoppema, M., Iversen, M.H., and Konrad, C.: Sea-ice derived meltwater stratification slows the biological carbon pump: results from continuous observations, Nat. Commun., 12, 7309, https://doi.org/10.1038/s41467-021-26943-z, 2021.

Aumont, O., Éthé, C., Tagliabue, A., Bopp, L., and Gehlen, M.: PISCES-v2: an ocean biogeochemical model for carbon and ecosystem studies, Geosci. Model Dev., 8, 2465–2513, https://doi.org/10.5194/gmd-8-2465-2015, 2015.

Aumont, O., van Hulten, M., Roy-Barman, M., Dutay, J.C., Éthé, C., and Gehlen, M.: Variable reactivity of particulate organic matter in a global ocean biogeochemical model, Biogeosciences, 14, 2321–2341, https://doi.org/10.5194/bg-14-2321-2017, 2017.

Baaklini, G., El Hourany, R., Fakhri, M., Brajard, J., Issa, L., Fifani, G., and Mortier, L.: Surface circulation properties in the eastern Mediterranean emphasized using machine learning methods, Ocean Sci., 18, 1491–1505, https://doi.org/10.5194/os-18-1491-2022, 2022.

Bachman, S.D.: The GM+E closure: A framework for coupling backscatter with the Gent and McWilliams parameterization, Ocean Model., 136, 85–106, https://doi.org/10.1016/j.ocemod.2019.02.00, 2019.

Baker, C.A., Martin, A.P., Yool, A., and Popova, E.: Biological carbon pump sequestration efficiency in the North Atlantic: A leaky or a long-term sink? Glob. Biogeochem. Cycles., 36, e2021GB007286, https://doi.org/10.1029/2021GB007286, 2022.

Barnier, B., Madec, G., Penduff, T., Molines, J.M., Treguier, A.M., Le Sommer, J., Beckmann, A., Biastoch, A., Böning, C., Dengg, J., Derval, C., Durand, E., Gulev, S., Remy, E., Talandier, C., Theetten, S., Maltrud, M., McClean, J., and De Cuevas B.: Impact of partial steps and momentum advection schemes in a global ocean circulation model at eddy-permitting resolution, Ocean Dyn., 56, 543–567, https://doi.org/10.1007/s10236-006-0082-1, 2006.

Bellacicco, M., Marullo, S., Dall'Olmo, G., Iudicone, D., and Buongiorno Nardelli, B.: The oceanic physical injection pump of organic carbon. Nat. Commun., 16, 7100, https://doi.org/10.1038/s41467-025-62363-z, 2025.

Berelson, W.M.: The Flux of Particulate Organic Carbon Into the Ocean Interior, Oceanography, 14, 59–67, https://www.jstor.org/stable/43924965, 2001.

Bianchi, D., Galbraith, E.D., Carozza, D.A., Mislan, K.A.S., and Stock, C.A.: Intensification of open-ocean oxygen depletion by vertically migrating animals, Nature Geosci., 6, 545–548, https://doi.org/10.1038/ngeo1837, 2013.

Biastoch, A., Schwarzkopf, F.U., Getzlaff, K., Rühs, S., Martin, T., Scheinert, M., Schulzki, T., Handmann, P., Hummels, R., and Böning, C.W.: Regional imprints of changes in the Atlantic Meridional Overturning Circulation in the eddy-rich ocean model VIKING20X, Ocean Sci., 17, 1177–1211, https://doi.org/10.5194/os-17-1177-2021, 2021.

Bishop, J.K.B., Conte, M.H., Wiebe, P.H., Roman, M.R., and Langdon, C.: Particulate matter production and consumption in deep mixed layers: observations in a warm-core ring, Deep Sea Research Part A. Oceanographic Research Papers, 33, 1813–1841, https://doi.org/10.1016/0198-0149(86)90081-6, 1986.

Bishop, J.K.: Autonomous Observations of the Ocean Biological Carbon Pump, Oceanography, 22, 182–193, https://www.jstor.org/stable/24860969, 2009.

Böning, C.W., Wagner, P., Handmann, P., Schwarzkopf, F.U., Getzlaff, K., and Biastoch, A.: Decadal changes in Atlantic overturning due to the excessive 1990s Labrador Sea convection, Nat. Commun., 14, 4635, https://doi.org/10.1038/s41467-023-40323-9, 2023.

Bopp, L., Resplandy, L., Orr, J.C., Doney, S.C., Dunne, J.P., Gehlen, M., Halloran, P., Heinze, C., Ilyina, T., Seferian, R., and Tjiputra, J.: Multiple stressors of ocean ecosystems in the 21st century: projections with CMIP5 models, Biogeosciences, 10, 6225–6245, https://doi.org/10.5194/bg-10-6225-2013, 2013.

Bol, R., Henson, S.A., Rumyantseva, A., and Briggs, N.: High-frequency variability of small-particle carbon export flux in the Northeast Atlantic, Glob. Biogeochem. Cycles, 32, 1803–1814, https://doi.org/10.1029/2018GB005963, 2018.

Boyd, P.W., Claustre, H., Levy, M., Siegel, D.A., and Weber, T.: Multi-faceted particle pumps drive carbon sequestration in the ocean, Nature, 568, 327–335, https://doi.org/10.1038/s41586-019-1098-2, 2019.

de Boyer Montégut, C.: Mixed layer depth over the global ocean : a climatology computed with a density threshold criterion of 0.03 kg/m3 from the value at the reference depth of 5 m, SEANOE [data set], https://doi.org/10.17882/98226, 2024.

Chen, S.M., Dezutter, T., Cote, D., Lalande, C., Edinger, E., and Sherwood, O.A.: Sea-ice-associated algae and zooplankton fecal pellets fuel organic particle export in the seasonally ice-covered northwestern Labrador Sea, Biogeosciences, 22, 2517–2540, https://doi.org/10.5194/bg-22-2517-2025, 2025.

Childress, J.J., Taylor, S.M., Cailliet, G.M., and Price, M.H.: Patterns of growth, energy utilization and reproduction in some meso- and bathypelagic fishes off Southern California, Mar. Biol., 61, 27–40, https://doi.org/10.1007/BF00410339, 1980.

Le Chevère, S., Dufour, C.O., Bopp, L., and Lévy, M.: Physical processes driving carbon subduction in the Southern Ocean in an eddy-permitting model, Glob. Biogeochem. Cycles, 40, e2024GB008416, https://doi.org/10.1029/2024GB008416, 2026.

Comiso, J.C.: Bootstrap Sea Ice Concentrations from Nimbus-7 SMMR and DMSP SSM/I-SSMIS (NSIDC-0079, Version 3), NASA National Snow and Ice Data Center Distributed Active Archive Center [data set], https://doi.org/10.5067/7Q8HCCWS4I0R, 2017.

Couespel, D., Lévy, M., and Bopp, L.: Oceanic primary production decline halved in eddy-resolving simulations of global warming, Biogeosciences, 18, 4321–4349, https://doi.org/10.5194/bg-18-4321-2021, 2021.

Dall'Olmo, G., Dingle, J., Polimene, L., Brewin, R.J., and Claustre, H.: Substantial energy input to the mesopelagic ecosystem from the seasonal mixed-layer pump, Nature Geosci., 9, 820–823, https://doi.org/10.1038/ngeo2818, 2016.

Davison, P.C., Checkley Jr, D.M., Koslow, J.A., and Barlow, J.: Carbon export mediated by mesopelagic fishes in the northeast Pacific Ocean, 116, 14–30, https://doi.org/10.1016/j.pocean.2013.05.013, 2013.

Debreu, L., Vouland, C., and Blayo, E.: AGRIF: Adaptive grid refinement in Fortran, Comput. Geosci., 34, 8–13, https://doi.org/10.1016/j.cageo.2007.01.009, 2008.

DeVries, T. and Weber, T.: The export and fate of organic matter in the ocean: New constraints from combining satellite and oceanographic tracer observations, Global Biogeochem. Cycles, 31, 535–555, https://doi.org/10.1002/2016GB005551, 2017.

Doléac, S., Lévy, M., El Hourany, R., and Bopp, L.: Toward more robust net primary production projections in the North Atlantic Ocean, Biogeosciences, 22, 841–862, https://doi.org/10.5194/bg-22-841-2025, 2025.

El Hourany, R., Mejia, C., Faour, G., Crépon, M., and Thiria, S.: Evidencing the impact of climate change on the phytoplankton community of the Mediterranean Sea through a bioregionalization approach, J. Geophys. Res.: Oceans, 126, e2020JC016808, https://doi.org/10.1029/2020JC016808, 2021.

Falkowski, P., Scholes, R.J., Boyle, E.E.A., Canadell, J., Canfield, D., Elser, J., Gruber, N., Hibbard, K., Högberg, P., Linder, S., and Mackenzie, F.T.: The Global Carbon Cycle: A Test of Our Knowledge of Earth as a System, Science, 290, 291–296, https://doi.org/10.1126/science.290.5490.291, 2000.

Fichefet, T. and Maqueda, M.M.: Sensitivity of a global sea ice model to the treatment of ice thermodynamics and dynamics, J. Geophys. Res., 102, 12609–12646, https://doi.org/10.1029/97JC00480, 1997.

https://doi.org/10.5194/egusphere-2026-4891
Preprint. Discussion started: 28 September 2026

Fogaren, K.E., Palevsky, H.I., Yoder, M.F., Nicholson, D., Cuevas, J.M., and Wanzer, L.: Winter mixing controls carbon sequestration by the biological pump in the subpolar North Atlantic, ESS Open Archive, https://doi.org/10.22541/essoar.176460522.25112894/v1, 2025.

Fontela, M., García-Ibáñez, M.I., Hansell, D.A., Mercier, H., and Pérez, F.F.: Dissolved Organic Carbon in the North Atlantic Meridional Overturning Circulation, Sci. Rep., 6, 26931, https://doi.org/10.1038/srep26931, 2016.

Fortin, A.S., Dufour, C.O., Merlis, T.M., and Msadek, R.: Geostrophic and Mesoscale Eddy Contributions to the Atlantic Meridional Overturning Circulation Decline under CO_2 Increase in the GFDL CM2-O Model Suite, J. Clim., 36, 6481–6498, https://doi.org/10.1175/JCLI-D-22-0561.1, 2023.

Fox, J., Behrenfeld, M.J., Halsey, K.H., and Graff, J.R.: Global estimates of particulate organic carbon concentration from the surface ocean to the base of the mesopelagic, Glob. Biogeochem. Cycles, 38, e2024GB008149, https://doi.org/10.1029/2024GB008149, 2024.

Fraser, N.J., Fox, A.D., Cunningham, S.A., Rath, W., Schwarzkopf, F.U., and Biastoch, A.: Vertical Velocity Dynamics in the North Atlantic and Implications for AMOC, J. Phys. Oceanogr., 54, 2011–2024, https://doi.org/10.1175/JPO-D-23-0229.1, 2024.

Gent, P.R., Willebrand, J., McDougall, T.J., and McWilliams, J.C.: Parameterizing Eddy-Induced Tracer Transports in Ocean Circulation Models, J. Phys. Oceanogr., 25, 463–474, https://doi.org/10.1175/1520-0485(1995)025<0463:PEITTI>2.0.CO;2, 1995.

Giering, S.L.C., Sanders, R., Martin, A.P., Lindemann, C., Möller, K.O., Daniels, C.J., Mayor, D.J., and St. John, M.A.: High export via small particles before the onset of the North Atlantic spring bloom, J. Geophys. Res. Oceans, 121, 6929–6945, https://doi.org/10.1002/2016JC012048, 2016.

Giering, S.L., Sanders, R., Martin, A.P., Henson, S.A., Riley, J.S., Marsay, C.M., and Johns, D.G.: Particle flux in the oceans: Challenging the steady state assumption, Global Biogeochem. Cycles, 31, 159–171, https://doi.org/10.1002/2016GB005424, 2017.

Gray, P.C., Savelyev, I., Cassar, N., Lévy, M., Boss, E., Lehahn, Y., Bourdin, G., Thompson, K.A., Windle, A., Gronniger, J., and Floge, S.: Evidence for kilometer-scale biophysical features at the Gulf Stream front, J. Geophys. Res.: Oceans, 129, e2023JC020526, https://doi.org/10.1029/2023JC020526, 2024.

Guidi, L., Legendre, L., Reygondeau, G., Uitz, J., Stemmann, L., and Henson, S.A.: A new look at ocean carbon remineralization for estimating deepwater sequestration, Global Biogeochem. Cycles, 29, 1044–1059, https://doi.org/10.1002/2014GB005063, 2015.

Haëck, C., Lévy, M., Mangolte, I., and Bopp, L.: Satellite data reveal earlier and stronger phytoplankton blooms over fronts in the Gulf Stream region, Biogeosciences, 20, 1741–1758, https://doi.org/10.5194/bg-20-1741-2023, 2023.

Hallberg, R.: Using a resolution function to regulate parameterizations of oceanic mesoscale eddy effects, Ocean Model., 72, 92–103, https://doi.org/10.1016/j.ocemod.2013.08.007, 2013.

Hansell, D.A.: Recalcitrant Dissolved Organic Carbon Fractions, Annu. Rev. Mar. Sci., 5, 421–445, https://doi.org/10.1146/annurev-marine-120710-100757, 2013.

Hansell, D.A. and Orellana, M.V.: Dissolved Organic Matter in the Global Ocean: A Primer, Gels, 7, 128, https://doi.org/10.3390/gels7030128, 2021.

Henson, S.A., Sanders, R., Madsen, E., Morris, P.J., Le Moigne, F., and Quartly, G.D.: A reduced estimate of the strength of the ocean's biological carbon pump, Geophys. Res. Lett., 38, L04606, https://doi.org/10.1029/2011GL046735, 2011.

Henson, S.A., Sanders, R., and Madsen, E.: Global patterns in efficiency of particulate organic carbon export and transfer to the deep ocean, Global Biogeochem. Cycles, 26, GB1028, https://doi.org/10.1029/2011GB004099, 2012.

Hewitt, H.T., Bell, M.J., Chassignet, E.P., Czaja, A., Ferreira, D., Griffies, S.M., Hyder, P., McClean, J.L., New, A.L., and Roberts, M.J.: Will high-resolution global ocean models benefit coupled predictions on short-range to climate timescales? Ocean Model., 120, 120–136, https://doi.org/10.1016/j.ocemod.2017.11.002, 2017.

Hewitt, H.T., Roberts, M., Mathiot, P., Biastoch, A., Blockley, E., Chassignet, E.P., Fox-Kemper, B., Hyder, P., Marshall, D.P., Popova, E., and Treguier, A.M.: Resolving and Parameterising the Ocean Mesoscale in Earth System Models, Curr. Clim. Change Rep., 6, 137–152, https://doi.org/10.1007/s40641-020-00164-w, 2020.

Hewitt, H., Fox-Kemper, B., Pearson, B., Roberts, M., and Klocke, D.: The small scales of the ocean may hold the key to surprises, Nat. Clim. Chang., 12, 496–499, https://doi.org/10.1038/s41558-022-01386-6, 2022.

Honjo, S. and Manganini, S.J.: Annual biogenic particle fluxes to the interior of the North Atlantic Ocean; studied at 34°N 21°W and 48°N 21°W, Deep Sea Research Part II: Topical Studies in Oceanography, 40, 587–607, https://doi.org/10.1016/0967-0645(93)90034-K, 1993.

Jansen, M.F., Adcroft, A.J., Hallberg, R., and Held, I.M.: Parameterization of eddy fluxes based on a mesoscale energy budget, Ocean Model., 92, 28–41, https://doi.org/10.1016/j.ocemod.2015.05.007, 2015.

Jansen, M.F., Held, I.M., Adcroft, A., and Hallberg, R.: Energy budget-based backscatter in an eddy permitting primitive equation model, Ocean Model., 94, 15–26, https://doi.org/10.1016/j.ocemod.2015.07.015, 2015.

Powell, J.R. and Ohman, M.D.: Use of glider-class acoustic Doppler profilers for estimating zooplankton biomass, J. Plankton Res., 34, 563–568, https://doi.org/10.1093/plankt/fbs023, 2012.

Johnson, A.R. and Omand, M.M.: Evolution of a subducted carbon-rich filament on the edge of the North Atlantic Gyre, J. Geophys. Res.: Oceans, 126, e2020JC016685, https://doi.org/10.1029/2020JC016685, 2021.

Johnson, L., Siegel, D.A., Thompson, A.F., Fields, E., Erickson, Z.K., Cetinic, I., Lee, C.M., D'Asaro, E.A., Nelson, N.B., Omand, M.M., and Sten, M.: Assessment of oceanographic conditions during the North Atlantic EXport processes in the ocean from RemoTe sensing (EXPORTS) field campaign, Prog. Oceanogr., 220, 103170, https://doi.org/10.1016/j.pocean.2023.103170, 2024.

Jónasdóttir, S.H., Visser, A.W., Richardson, K., and Heath, M.R.: Seasonal copepod lipid pump promotes carbon sequestration in the deep North Atlantic, Proc. Natl. Acad. Sci., 112, 12122–12126, https://doi.org/10.1073/pnas.1512110112, 2015.

Jouini, M., Béranger, K., Arsouze, T., Beuvier, J., Thiria, S., Crépon, M., and Taupier-Letage, I.: The Sicily Channel surface circulation revisited using a neural clustering analysis of a high-resolution simulation, J. Geophys. Res. Oceans, 121, 4545–4567, https://doi.org/10.1016/10.1002/2015JC011472, 2016.

Karleskind, P., Lévy, M., and Mémery, L.: Subduction of carbon, nitrogen, and oxygen in the northeast Atlantic, J. Geophys. Res., 116, C02025, https://doi.org/10.1029/2010JC006446, 2011.

Keutgen De Greef, M., Resplandy, L., and Poupon, M.A.: Global eddy subduction carbon pump from Argo floats, Glob. Biogeochem. Cycles, 40, e2025GB008912, https://doi.org/10.1029/2025GB008912, 2026.

Lacour, L., Briggs, N., Claustre, H., Ardyna, M., and Dall'Olmo, G.: The intraseasonal dynamics of the mixed layer pump in the subpolar North Atlantic Ocean: A Biogeochemical-Argo float approach, Glob. Biogeochem. Cycles, 33, 266–281, https://doi.org/10.1029/2018GB005997, 2019.

Laine, M., Kulk, G., Jönsson, B.F., and Sathyendranath, S.: A machine learning model-based satellite data record of dissolved organic carbon concentration in surface waters of the global open ocean, Front. Mar. Sci., 11, 1305050, https://doi.org/10.3389/fmars.2024.1305050, 2024.

Lemaitre, N., Planchon, F., Planquette, H., Dehairs, F., Fonseca-Batista, D., Roukaerts, A., Deman, F., Tang, Y., Mariez, C., and Sarthou, G.: High variability of particulate organic carbon export along the North Atlantic GEOTRACES section GA01 as deduced from ^{234}Th fluxes, Biogeosciences, 15, 6417–6437, https://doi.org/10.5194/bg-15-6417-2018, 2018.

Leonelli, F.E., Bellacicco, M., Pitarch, J., Organelli, E., Buongiorno Nardelli, B., De Toma, V., Cammarota, C., Marullo, S., and Santoleri, R.: Ultra-oligotrophic waters expansion in the North Atlantic Subtropical Gyre revealed by 21 years of satellite observations, Geophys. Res. Lett., 49, e2021GL096965, https://doi.org/10.1029/2021GL096965, 2022.

Lévy, M., Klein, P., and Treguier, A.M.: Impact of sub-mesoscale physics on production and subduction of phytoplankton in an oligotrophic regime, J. Mar. Res., 59, https://elischolar.library.yale.edu/journal_of_marine_research/2401, 2001.

Lévy, M.: Mesoscale variability of phytoplankton and of new production: Impact of the large-scale nutrient distribution, J. Geophys. Res., 108, 3358, http://doi.org/10.1029/2002JC001577, 2003.

Lévy, M., Klein, P., Tréguier, A.M., Iovino, D., Madec, G., Masson, S., and Takahashi, K.: Modifications of gyre circulation by sub-mesoscale physics, Ocean Model., 34, 1–15, https://doi.org/10.1016/j.ocemod.2010.04.001, 2010.

Lévy, M., Ferrari, R., Franks, P.J., Martin, A.P., and Rivière, P.: Bringing physics to life at the submesoscale, Geophys. Res. Lett., 39, L14602, https://doi.org/10.1029/2012GL052756, 2012.

Lévy, M., Iovino, D., Resplandy, L., Klein, P., Madec, G., Tréguier, A.M., Masson, S., and Takahashi, K.: Large-scale impacts of submesoscale dynamics on phytoplankton: Local and remote effects, Ocean Model., 43, 77–93, https://doi.org/10.1016/j.ocemod.2011.12.003, 2012.

Lévy, M., Bopp, L., Karleskind, P., Resplandy, L., Éthé, C., and Pinsard, F.: Physical pathways for carbon transfers between the surface mixed layer and the ocean interior, Global Biogeochem. Cycles, 27, 1001–1012, https://doi.org/10.1002/gbc.20092, 2013.

Lévy, M., Franks, P.J., and Smith, K.S.: The role of submesoscale currents in structuring marine ecosystems, Nat. Commun., 9, 4758, https://doi.org/10.1038/s41467-018-07059-3, 2018.

Lévy, M., Couespel, D., Haëck, C., Keerthi, M.G., Mangolte, I., and Prend, C.J.: The Impact of Fine-Scale Currents on Biogeochemical Cycles in a Changing Ocean, Annu. Rev. Mar. Sci., 16, 191–215, https://doi.org/10.1146/annurev-marine-020723-020531, 2024.

Lloyd, S.: Least squares quantization in PCM, IEEE transactions on information theory, 28, 129–137, https://doi.org/10.1109/TIT.1982.1056489, 1982.

Locarnini, R.A., Mishonov, A.V., Antonov, J.I., Boyer, T.P., Garcia, H.E., Baranova, O.K., Zweng, M.M., Paver, C.R., Reagan, J., Johnson, D.R., Hamilton, M., Seidov, D., Levitus, S.: World ocean atlas 2013. Volume 1, Temperature, NOAA atlas NESDIS 73, http://doi.org/10.7289/V55X26VD, 2013.

Longhurst, A.R.: Ecological geography of the sea, Elsevier, https://books.google.fr/books?hl=en&lr=&id=QdJZezzrCfQC&oi=fnd&pg=PP1&ots=4NPzxVMTxU&sig=0iK7X65sX0D80_gkEaaVveWVcXY&redir_esc=y#v=onepage&q&f=false, 2010.

Madec, G., Bourdallé-Badie, R., Bouttier, P.A., Bricaud, C., Bruciaferri, D., Calvert, D., Chanut, J., Clementi, E., Coward, A., Delrosso, D., Ethé, C., Flavoni, S., Graham, T., Harle, J., Iovino, D., Lea, D., Lévy, C., Lovato, T., Martin, N., Masson, S., Mocavero, S., Paul, J., Rousset, C., Storkey, D., Storto, A., and Vancoppenolle, M.: NEMO ocean engine (Version v3.6-patch), Notes du Pôle de modélisation de l'Institut Pierre-Simon Laplace (IPSL), https://doi.org/10.5281/zenodo.3248739, 2016.

Mahadevan, A.: The Impact of Submesoscale Physics on Primary Productivity of Plankton. Annual Review Marine Science, Annu. Rev. Mar. Sci., 8, 161–184, https://doi.org/10.1146/annurev-marine-010814-015912, 2016.

Mak, J., Maddison, J.R., Marshall, D.P., and Munday, D.R.: Implementation of a Geometrically Informed and Energetically Constrained Mesoscale Eddy Parameterization in an Ocean Circulation Model, J. Phys. Oceanogr., 48, 2363–2382, https://doi.org/10.1175/JPO-D-18-0017.1, 2018.

Mak, J., Maddison, J.R., Marshall, D.P., Ruan, X., Wang, Y., and Yeow, L.: Scale-awareness in an eddy energy constrained mesoscale eddy parameterization, J. Adv. Model. Earth Syst., 15, e2023MS003886, https://doi.org/10.1029/2023MS003886, 2023.

https://doi.org/10.5194/egusphere-2026-4891
Preprint. Discussion started: 28 September 2026

Marshall, J., Scott, J.R., Romanou, A., Kelley, M, and Leboissetier, A.: The dependence of the ocean's MOC on mesoscale eddy diffusivities: A model study, Ocean Model., 111, 1–8, https://doi.org/10.1016/j.ocemod.2017.01.001, 2017.

Martin, J.H., Knauer, G.A., Karl, D.M., and Broenkow, W.W.: VERTEX: carbon cycling in the northeast Pacific, Deep-Sea Res., Part A, Oceanogr. Res. Pap., 34, 67–285, https://doi.org/10.1016/0198-0149(87)90086-0, 1987.

McClain, C.R., Signorini, S.R., and Christian, J.R.: Subtropical gyre variability observed by ocean-color satellites, Deep-Sea Res. II: Top. Stud. Oceanogr., 51, 281–301, https://doi.org/10.1016/j.dsr2.2003.08.002, 2004.

McGillicuddy Jr, D.J., Resplandy, L., and Lévy, M.: Estimating particle export flux from satellite observations: Challenges associated with spatial and temporal decoupling of production and export, J. Mar. Res., 77, https://elischolar.library.yale.edu/journal_of_marine_research/479, 2019.

McQueen, J.B.: Some Methods for Classification and Analysis of Multivariate Observations, Proceedings of the 5th Berkeley Symposium on Mathematical Statistics and Probability, Volume 1: Statistics, University of California Press, Berkeley, 281–297, http://projecteuclid.org/euclid.bsmsp/1200512992, 1967.

Le Moigne, F.A., Henson, S.A., Sanders, R.J., and Madsen, E.: Global database of surface ocean particulate organic carbon export fluxes diagnosed from the ^{234}Th technique, Earth Syst. Sci. Data, 5, 295–304, https://doi.org/10.5194/essd-5-295-2013, 2013.

Le Moigne, F.A.: Pathways of Organic Carbon Downward Transport by the Oceanic Biological Carbon Pump, Front. Mar. Sci., 6, 634, https://doi.org/10.3389/fmars.2019.00634, 2019.

Nowicki, M., DeVries, T., and Siegel, D.A.: Quantifying the carbon export and sequestration pathways of the ocean's biological carbon pump, Glob. Biogeochem. Cycles, 36, e2021GB007083, https://doi.org/10.1029/2021GB007083, 2022.

Nowicki, M., DeVries, T., and Siegel, D.A.: The influence of air-sea CO_2 disequilibrium on carbon sequestration by the ocean's biological pump, Glob. Biogeochem. Cycles, 38, e2023GB007880, https://doi.org/10.1029/2023GB007880, 2024.

Omand, M.M., D'Asaro, E.A., Lee, C.M., Perry, M.J., Briggs, N., Cetinić, I., and Mahadevan, A.: Eddy-driven subduction exports particulate organic carbon from the spring bloom, Science, 348, 222–225, https://doi.org/10.1126/science.1260062, 2015.

Palevsky, H.I. and Nicholson, D.P.: The North Atlantic Biological Pump: INSIGHTS FROM THE OCEAN OBSERVATORIES INITIATIVE IRMINGER SEA ARRAY, Oceanography, 31, 42–49, http://www.jstor.org/stable/26307786, 2018.

Palevsky, H.I. and Doney, S.C.: Sensitivity of 21st century ocean carbon export flux projections to the choice of export depth horizon, Glob. Biogeochem. Cycles, 35, e2020GB006790, https://doi.org/10.1029/2020GB006790, 2021.

Reagan, J.R., Garcia, H.E., Boyer, T.P., Baranova, O.K., Bouchard, C., Cross, S.L., Dukhovskoy, D., Grodsky, A., Locarnini, R.A., Mishonov, A.V., and Paver, C.R.: World Ocean Atlas 2023: Product Documentation, https://doi.org/10.25923/a78k-gq49, 2023.

Redi, M.H.: Oceanic Isopycnal Mixing by Coordinate Rotation, J. Phys. Oceanogr., 12, 1154–1158, https://doi.org/10.1175/1520-0485(1982)012<1154:OIMBCR>2.0.CO;2, 1982.

Resplandy, L., Lévy, M., and McGillicuddy Jr, D.J.: Effects of eddy-driven subduction on ocean biological carbon pump, Glob. Biogeochem. Cycles, 33, 1071–1084, https://doi.org/10.1029/2018GB006125, 2019.

Reynolds, D.: Gaussian mixture models, Encycl. Biometrics, Springer, Boston, MA., https://doi.org/10.1007/978-1-4899-7488-4_196, 2015.

Romanelli, E., Giering, S.L.C., Estapa, M., Siegel, D.A., and Passow, U.: Can intense storms affect sinking particle dynamics after the North Atlantic spring bloom? Limnol. Oceanogr., 69, 2963–2974, https://doi.org/10.1002/lno.12723, 2024.

Ruan, X., Couespel, D., Lévy, M., Li, J., Mak, J., and Wang, Y.: Combined physical and biogeochemical assessment of mesoscale eddy parameterisations in ocean models: Eddy induced advection at non-eddying resolutions, Ocean Model., 183, 102204, https://doi.org/10.1016/j.ocemod.2023.102204, 2023.

https://doi.org/10.5194/egusphere-2026-4891
Preprint. Discussion started: 28 September 2026

Ruan, X., Couespel, D., Lévy, M., Li, J., Mak, J., and Wang, Y.: Combined physical and biogeochemical assessment of mesoscale eddy parameterisations in ocean models: Eddy-induced advection at eddy-permitting resolutions, Ocean Model., 190, 102396, https://doi.org/10.1016/j.ocemod.2024.102396, 2024.

Rühs, S., Oliver, E.C., Biastoch, A., Böning, C.W., Dowd, M., Getzlaff, K., Martin, T., and Myers, P.G.: Changing spatial patterns of deep convection in the subpolar North Atlantic, J. Geophys. Res.: Oceans, 126, e2021JC017245, https://doi.org/10.1029/2021JC017245, 2021.

Sanders, R., Henson, S.A., Koski, M., De La Rocha, C.L., Painter, S.C., Poulton, A.J., Riley, J., Salihoglu, B., Visser, A., Yool, A., and Bellerby, R.: The Biological Carbon Pump in the North Atlantic, Prog. Oceanogr., 129, 200–218, https://doi.org/10.1016/j.pocean.2014.05.005, 2014.

Schiller-Weiss, I., Schulzki, T., Schwarzkopf, F.U., Martin, T., and Biastoch, A.: Sea Surface Height Response to Decadal-Scale AMOC Changes in an Eddy-Rich Ocean Model, J. Clim., 38, 5265–5283, https://doi.org/10.1175/JCLI-D-24-0646.1, 2025.

Schulzki, T., Schwarzkopf, F.U., and Biastoch, A.: An Atlantic-wide assessment of marine heatwaves beyond the surface in an eddy-rich ocean model, Ocean Sci., 21, 2481–2504, https://doi.org/10.5194/os-21-2481-2025, 2025.

Siegel, D.A., Buesseler, K.O., Doney, S.C., Sailley, S.F., Behrenfeld, M.J., and Boyd, P.W.: Global assessment of ocean carbon export by combining satellite observations and food-web models, Global Biogeochem. Cycles, 28, 181–196, https://doi.org/10.1002/2013GB004743, 2014.

Siegel, D.A., DeVries, T., Cetinić, I., and Bisson, K.M.: Quantifying the Ocean's Biological Pump and Its Carbon Cycle Impacts on Global Scales, Annual review of marine science, 15, 329–356, https://doi.org/10.1146/annurev-marine-040722-115226, 2023.

Stramska, M.: The diffusive component of particulate organic carbon export in the North Atlantic estimated from SeaWiFS ocean color, Deep Sea Research Part I: Oceanographic Research Papers, 57, 284–296, https://doi.org/10.1016/j.dsr.2009.11.007, 2010.

Szekely, T., Gourrion, J., Pouliquen, S., Reverdin, G., and Merceur, F.: CORA, Coriolis Ocean Dataset for Reanalysis [data set], https://doi.org/10.17882/46219, 2019.

Terhaar, J., Orr, J.C., Gehlen, M., Ethé, C., and Bopp, L.: Model constraints on the anthropogenic carbon budget of the Arctic Ocean, Biogeosciences, 16, 2343–2367, https://doi.org/10.5194/bg-16-2343-2019, 2019.

Treguier, A.M., de Boyer Montégut, C., Bozec, A., Chassignet, E.P., Fox-Kemper, B., McC. Hogg, A., Iovino, D., Kiss, A.E., Le Sommer, J., Li, Y., and Lin, P.: The mixed-layer depth in the Ocean Model Intercomparison Project (OMIP): impact of resolving mesoscale eddies, Geosci. Model. Dev., 16, 3849–3872, https://doi.org/10.5194/gmd-16-3849-2023, 2023.

Tsujino, H., Urakawa, S., Nakano, H., Small, R.J., Kim, W.M., Yeager, S.G., Danabasoglu, G., Suzuki, T., Bamber, J.L., Bentsen, M., and Böning, C.W.: JRA-55 based surface dataset for driving ocean–sea-ice models (JRA55-do), Ocean Model., 130, 79–139, https://doi.org/10.1016/j.ocemod.2018.07.002, 2018.

Vatanen, T., Osmala, M., Raiko, T., Lagus, K., Sysi-Aho, M., Orešič, M., Honkela, T., and Lähdesmäki, H.: Self-organization and missing values in SOM and GTM, Neurocomputing, 147, 60–70, https://doi.org/10.1016/j.neucom.2014.02.061, 2015.

Volk, T. and Hoffert, M.I.: Ocean Carbon Pumps: Analysis of Relative Strengths and Efficiencies in Ocean-Driven Atmospheric CO_2 Changes, The Carbon Cycle and Atmospheric CO_2: Natural Variations Archean to Present, 32, 99–110, https://doi.org/10.1029/GM032p0099, 1985.

Wang, B. and Fennel, K.: Biogeochemical-Argo data suggest significant contributions of small particles to the vertical carbon flux in the subpolar North Atlantic. Limnol. Oceanogr., 67, 2405–2417, https://doi.org/10.1002/lno.12209, 2022.

https://doi.org/10.5194/egusphere-2026-4891
Preprint. Discussion started: 28 September 2026

Zweng, M.M., Reagan, J.R., Antonov, J.I., Locarnini, R.A., Mishonov, A.V., Boyer, T.P., Garcia, H.E., Baranova, O.K., Johnson, D.R., Seidov, D., Biddle, M.M., and Levitus, S.: World Ocean Atlas 2013, Volume 2: Salinity, NOAA Atlas NESDIS 74, http://doi.org/10.7289/V5251G4D, 2013.